A Tale of Two Channels

The 2003 Nobel Prize in Chemistry was awarded to Peter Agre and Rod McKinnon, for their work on the water channel (aquaporin) and the potassium channel, respectively. The fascinating stories of these proteins are told in the images shown here.

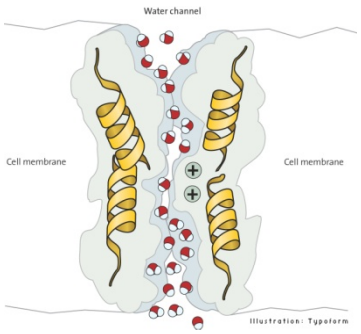

Aquaporin passes a single column of water,….while excluding protons.

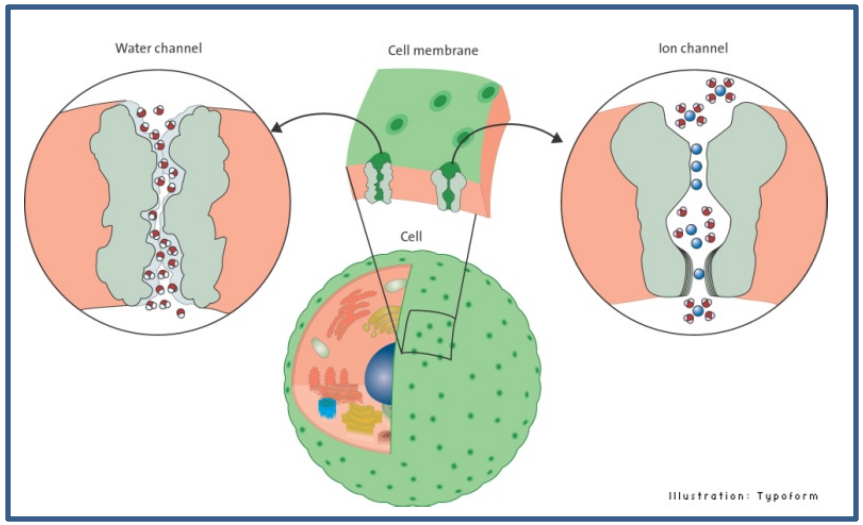

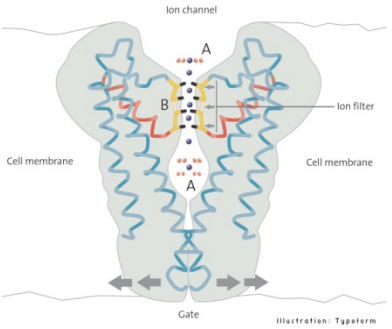

The K^+ channel --- very fast, and selective

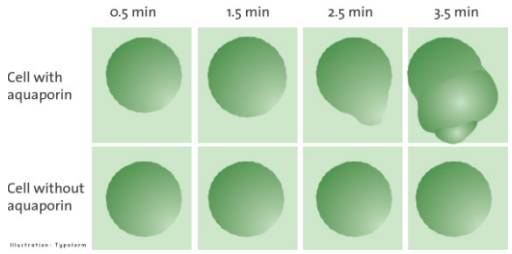

Exploding frog eggs…..

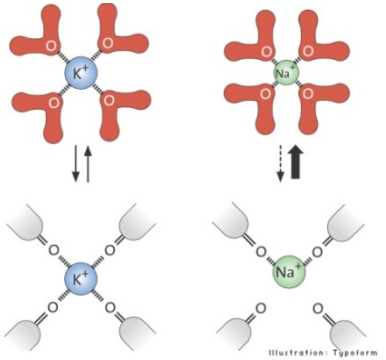

Dehydrating K^+ ions…..

Images taken from http://nobelprize.org/nobel_prizes/chemistry/laureates/2003/public.html

The Nobel Prize in Chemistry 2003

8 October 2003

All living matter is made up of cells. A single human being has as many as the stars in a galaxy, about one hundred thousand million. The various cells – e.g. muscle cells, kidney cells and nerve cells – act together in an intricate system in each one of us. Through pioneering discoveries concerning the water and ion channels of cells, this year's Nobel Laureates **Peter Agre** and **Roderick MacKinnon**, have contributed to fundamental chemical knowledge on how cells function. They have opened our eyes to a fantastic family of molecular machines: channels, gates and valves all of which are needed for the cell to function.

Molecular channels through the cell wall

To maintain even pressure in the cells it is important that water can pass through the cell wall. This has been known for a long time. The appearance and function of these pores, remained for a long time as one of the classical unsolved problems of biochemistry. It was not until around 1990 that Peter Agre discovered the first water channel. Like so much else in the living cell, it was all about a protein.

Water molecules are not the only entities that pass into and out of the cell. For thousands of millions of cells to be able to function as something other than one large lump, coordination is required. Thus communication between the cells is necessary. The signals sent in and between cells consist of ions or small molecules. These start cascades of chemical reactions that cause our muscles to tense, our eyes to water – indeed, that control all our bodily functions. The signals in our brains also involve such chemical reactions. When we stub a toe this starts a signal moving up towards the brain. Along a chain of nerve cells, through interaction between chemical signals and ion currents, information is conveyed from cell to cell like a baton in a relay race.

It was in 1998 that Roderick MacKinnon succeeded for the first time in showing what ion channels look like at atomic level – an achievement which, together with Agre's discovery of water channels, opened up entirely new research areas in biochemistry and biology.

The medical consequences of Agre's and MacKinnon's discoveries are also important. A number of diseases can be attributed to poor functioning in the water and ion channels of the human body. With the help of fundamental knowledge of what they look like and how they work, there are now new possibilities for developing new and more effective pharmaceuticals.

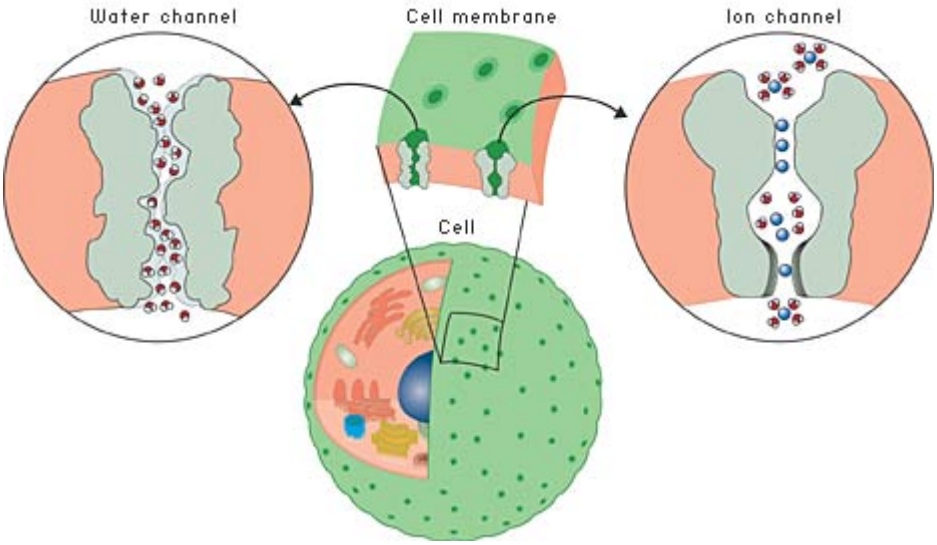

High resolution image (jpeg 210 kB) »

Fig 1. The dividing wall between the cell and the outside world – including other cells – is far from being an impervious shell. On the contrary, it is perforated by various channels. Many of these are specially adapted to one specific ion or molecule and do not permit any other type to pass. Here to the left we see a water channel and to the right an ion channel.

Water channels

The hunt for the water channels

As early as the middle of the nineteenth century it was understood that there must be openings in the cell membrane to permit a flow of water and salts. In the middle of the 1950s it was discovered that water can be rapidly transported into and out of cells through pores that admit water molecules only. During the next 30 years this was studied in detail and the conclusion was that there must be some type of selective filter that prevents ions from passing through the membrane while water molecules, which are uncharged, flow freely. Thousands of millions of water molecules per second pass through one single channel!

Although this was known, it was not until 1992 that anybody was able to identify what this molecular machinery really looked like; that is, to identify what protein or proteins formed the actual channel. In the mid-1980s Peter Agre studied various membrane proteins from the red blood cells. He also found one of these in the kidney. Having determined both its peptide sequence and the corresponding DNA sequence, he realised that this must be the protein that so many had sought before him: the cellular water channel.

Agre tested his hypothesis in a simple experiment (fig. 2) where he compared cells which contained the protein in question with cells which did not have it. When the cells were placed in a water solution, those that had the protein in their membranes absorbed water by osmosis and swelled up while those that lacked the protein were not affected at all. Agre also ran trials with artificial cells, termed liposomes, which are a type of soap bubble

surrounded on the outside and the inside by water. He found that the liposomes became permeable to water if the protein was planted in their membranes.

What is osmosis?

The liquid pressure in plant and animal cells is maintained through osmosis. In osmosis, small molecules (such as water) pass through a semi-permeable membrane. If the membrane does not admit macromolecules or salts that are in higher concentrations on one side of the membrane, the small molecules (water) will cross to this side, attempting to ”dilute” the substance that cannot pass through the membrane. The osmotic pressure thus arising is the reason why cells are often swollen and stiff, in a flower stalk, for example.

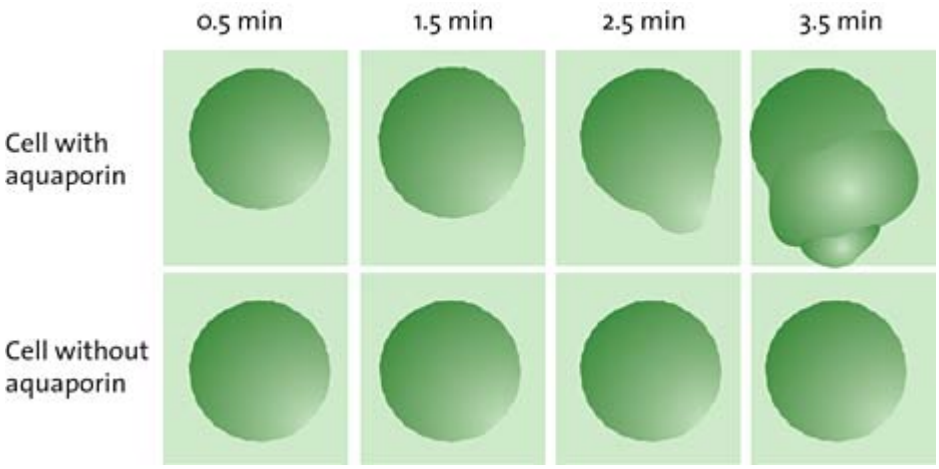

High resolution image (jpeg 165 kB) »

Fig 2. Peter Agre’s experiment with cells containing or lacking aquaporin. The aquaporin is necessary for making the cell absorb water and swell.

Peter Agre also knew that mercury ions prevent cells from taking up and releasing water, and he showed that water transport through his new protein was prevented in the same way by mercury. This made him even more sure of that he had discovered what was actually the water channel . Agre named the protein *aquaporin,* ”water pore”.

How does the water channel work? A question of form and function

In 2000, together with other research teams, Agre reported the first high-resolution images of the three-dimensional structure of the aquaporin. With these data, it was possible to map in detail how a water channel functions. How is it that it only admits water molecules and not other molecules or ions? The membrane is, for instance, not allowed to leak protons. This is crucial because the difference in proton concentration between the inside and the outside of the cell is the basis of the cellular energy-storage system.

Selectivity is a central property of the channel. Water molecules worm their way through the narrow channel by orienting themselves in the local electrical field formed by the atoms of the channel wall. Protons (or rather oxonium ions, H_3O^+) are stopped on the way and rejected because of their positive charges.

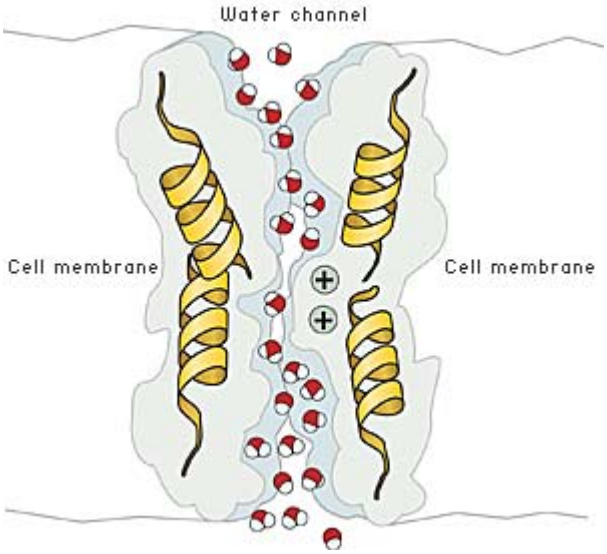

High resolution image (jpeg 173 kB) »

Animations »

Fig 3. Passage of water molecules through the aquaporin AQP1. Because of the positive charge at the center of the channel, positively charged ions such as H_3O^+, are deflected. This prevents proton leakage through the channel.

The medical significance of the water channels

During the past ten years, water channels have developed into a highly topical research field. The aquaporins have proved to be a large protein family. They exist in bacteria, plants and animals. In the human body alone, at least eleven different variants have been found.

The function of these proteins has now been mapped in bacteria and in plants and animals, with focus on their physiological role. In humans, the water channels play an important role in, among other organs, the kidneys.

The kidney is an ingenious apparatus for removing substances the body wishes to dispose of. In its windings (termed glomeruli), which function as a sieve, water, ions and other small molecules leave the blood as ‘primary’ urine. Over 24 hours, about 170 litres of primary urine is produced. Most of this is reabsorbed with a series of cunning mechanisms so that finally about one litre of urine a day leaves the body.

From the glomeruli, primary urine is passed on through a winding tube where about 70% of the water is reabsorbed to the blood by the aquaporin AQP1. At the end of the tube, another 10% of water is reabsorbed with a similar aquaporin, AQP2. Apart from this, sodium, potassium and chloride ions are also reabsorbed into the blood. Antidiuretic hormone (vasopressin) stimulates the transport of AQP2 to cell membranes in the tube walls and hence

increases the water resorption from the urine. People with a deficiency of this hormone might be affected by the disease *diabetes insipidus* with a daily urine output of 10-15 litres.

Ion channels

The cells signal with salt!

The first physical chemist, the German Wilhelm Ostwald (Nobel Prize in Chemistry 1909) proposed in 1890 that the electrical signals measured in living tissue could be caused by ions moving in and out through cell membranes. This electro-chemical idea rapidly achieved acceptance. The notion of the existence of some type of narrow ion channel arose in the 1920s. The two British scientists Alan Hodgkin and Andrew Huxley made a major breakthrough at the beginning of the 1950s and for this were awarded the Nobel Prize in Physiology or Medicine in 1963. They showed how ion transport through nerve cell membranes produces a signal that is conveyed from nerve cell to nerve cell like a relay race baton. It is primarily sodium and potassium ions, Na^+ and K^+, that are active in these reactions. Thus as much as fifty years ago there was well-developed knowledge of the central functions of the ion channels. They had to be able to admit one ion type selectively, but not another. Likewise, it had to be possible for the channels to open and shut and sometimes to conduct ions in one direction only. But how this molecular machinery really worked was long to remain a mystery.

Ion-selective channel

During the 1970s it was shown that the ion channels were able to admit only certain ions because they were equipped with some kind of ”ion filter”. Of particular interest was the finding of channels that admit potassium ions but not sodium ions – even though the sodium ion is smaller than the potassium ion. It was suspected that the oxygen atoms in the protein played an important role as “substitutes” for the water molecules with which the potassium ion surrounds itself in the water solution and from which it must free itself during entry to the channel. But further progress with this hypothesis was difficult – what was now needed was simply high-resolution pictures of the type only X-ray crystallography can provide. The problem was that it is extremely difficult to determine the structure of membrane proteins with this method, and the ion channels were no exception. Membrane proteins from plants and animals are more complicated and difficult to work with than those from bacteria. Using bacterial channel proteins that resemble human ion channels as closely as possible might perhaps offer a way forwards. Many researchers tried in vain. The breakthrough came from an unexpected direction. Roderick MacKinnon, after studying biochemistry, turned to medicine and qualified as medical doctor. After working as a physician for some years, he grew so interested in ion channels that he started to do research in the field: “My scientific career in effect began at the age of 30”, he has admitted. But his career took off quickly. Realising that better and higher-resolution structures were needed for understanding how ion channels function, he decided to learn the fundamentals of X-ray crystallography. It was then only a few years before he astonished the whole research community by presenting a structure of an ion channel. This was in April 1998.

First ion channel mapped – atom by atom

In 1998, then, MacKinnon determined the first high-resolution structure of an ion channel, called KcsA, from the bacterium *Streptomyces lividans.* MacKinnon revealed for the first time how an ion channel functions at atomic

level. The ion filter, which admits potassium ions and stops sodium ions, could now be studied in detail. Not only was it possible to unravel how the ions passed through the channel, they could also be seen in the crystal structure – surrounded by water molecules just before they enter the ion filter; right in the filter, and when they meet the water on the other side of the filter (fig. 4). MacKinnon could explain why potassium ions but not sodium ions are admitted through the filter: namely, because the distance between the potassium ion and the oxygen atoms in the filter is the same as that between the potassium ion and the oxygen atoms in the water molecules surrounding the potassium ion when it is outside the filter. Thus it can slide through the filter unopposed. However, the sodium ion, which is smaller than the potassium ion, can *not* pass through the channel. This is because it does not fit between the oxygen atoms in the filter and therefore remains in the water solution. The ability of the channel to strip the potassium ion of its water and allow it to pass at no cost in energy is a kind of selective catalysed ion transport.

The cell must also be able to control the opening and closing of ion channels. MacKinnon has shown that this is achieved by a gate at the bottom of the channel which opened and closed a molecular “sensor”. This sensor is situated close to the gate. Certain sensors react to certain signals, e.g. an increase in the concentration of calcium ions, an electric voltage over the cell membrane or binding of a signal molecule of some kind. By connecting different sensors to ion channels, nature has created channels that respond to a large number of different signals.

Fig 4. The ion channel permits passage of potassium ions but not sodium ions. The oxygen atoms of the ion filter form an environment very similar to the water environment outside the filter. The cell may also control opening and closing of the channel.

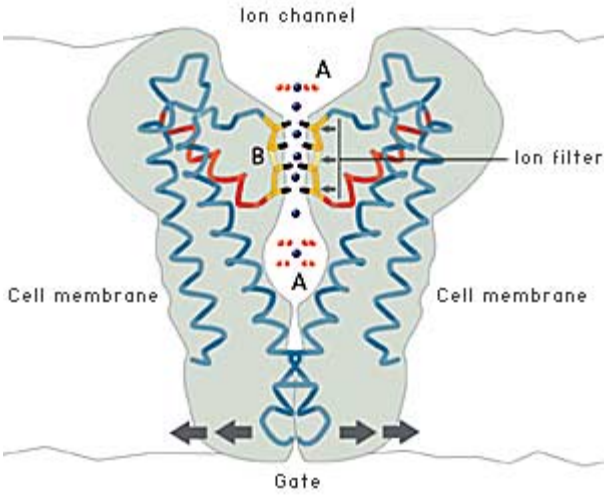

High resolution image (jpeg 137 kB) »

OUTSIDE THE ION FILTER (A)

Outside the cell membrane the ions are bound to water molecules with certain distances to the oxygen atoms of the water.

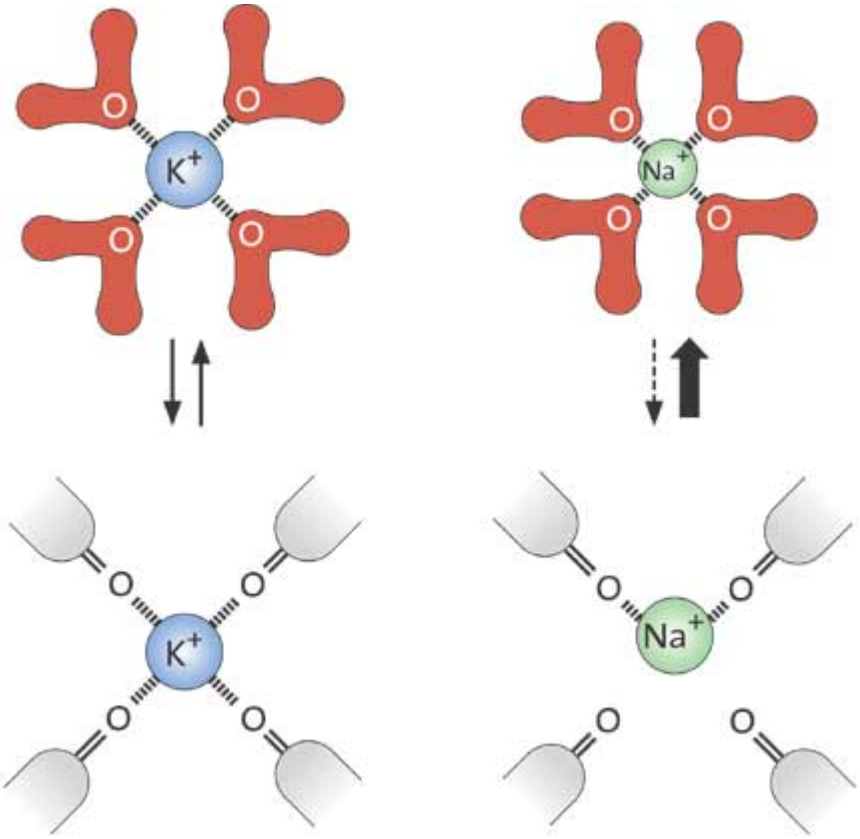

High resolution image (jpeg 121 kB) »

INSIDE THE ION FILTER (B)

For the potassium ions the distance to the oxygen atoms in the ion filter is the same as in water.

The sodium ions, which are smaller, do not fit in between the oxygen atoms in the filter. This prevents them from entering the channel.

Understanding diseases

Membrane channels are a precondition for all living matter. For this reason, increased understanding of their function constitutes an important basis for understanding many disease states. Dehydration of various types, and sensitivity to heat, are connected with the efficancy of the aquaporins. The European heat waves of recent years, for example, resulted in many deaths where the cause has sometimes been connected to problems in maintaining the body-fluid balance. In these processes the aquaporins are of crucial importance.

Disturbances in ion channel function can lead to serious diseases of the nervous system as well as the muscles, e.g. the heart. This makes the ion channels important drug targets for the pharmaceutical industry.

Links and further reading »

The Aquaporin Water Channels

Peter Agre

Johns Hopkins University School of Medicine, Baltimore, Maryland

The topic of my talk, the aquaporins, is something that we have been studying in our lab for the last 15 years. It is not something that I anticipated when starting my career. In fact, I am a hematologist, but in science, sometimes what we find is not what we are looking for. A typical middle-aged man, I weigh 75 kg, of which 50 are water. This is something that we all share. Water is the major component of all our cells in all of our tissues. This is also shared with all other life forms, other vertebrates, invertebrates, microorganisms, and plants. Water can be described as the "solvent of life"—without water, there is no life. Multicellular life comes with potential problems. One of these problems is the movement of fluids across biological barriers, and the principal barrier for most of our tissues is the plasma membrane. The aquaporins, which I will describe, are an answer to how water crosses biological membranes, but specific questions still need be defined. I am very pleased to be speaking to the American Thoracic Society because I believe that many of the questions related to fluid movements in lung are still unsettled.

When we began our studies some years back, the problem of membrane water permeability had already been looked at by a generation of biophysicists and physiologists. With the discovery of the lipid bilayer in the 1920s, it was speculated that a finite degree of water permeability would occur by simple diffusion through the plasma membrane. However, the work of very vigorous biophysicists and physiologists indicated that in certain tissues—for example, renal tubule, secretory glands, and red cells—the water permeability is much larger than could be explained through simple diffusion through the plasma membrane. And these investigators predicted correctly that there must be specialized water-selective channels in these membranes. The current view is that both mechanisms occur—diffusion through all membranes and flow through aquaporins that are present in certain special membranes. The biophysical differences are quite significant; diffusion is a low-capacity bidirectional movement of water, whereas water channels have a high capacity and great selectivity for water. The channels are so selective that water passes through them, and acid does not. As we all know, protons exist in fluid as the hydronium ion. This distinction is really quite important. Every day, our kidneys filter and reabsorb about 180 L of water. If we do not reabsorb that water, we would die of dehydration. If we reabsorb the water, along with protons, we would become systemically acidotic. The movement of water through the aquaporins is driven by osmotic gradients. For example, red cells dropped into seawater will shrink because water leaves the cells; red cells dropped into fresh water will swell and explode since water enters the cell. The process of osmosis that we all learned about as children is known to occur very rapidly in membranes in which aquaporins are present.

An experiment by Bob Macy at the University of California, Berkeley, in 1970 made a very important observation. It was known that diffusion of water through membranes is not inhibited by any known pharmacologic agents. Macy discovered that mercuric chloride reduces the water permeability of red cells, and when the membranes have been treated with reducing agents, the water permeability was restored. Macy concluded that the water channel protein must contain a free sulfhydryl somewhere within the pore. This provided very strong evidence that water channels must exist; however, most physiologists and other scientists remained very skeptical. They could not identify water channel molecules, much less purify them, clone them, express them, or reconstitute them.

Our laboratory got into the water channel field by accident. We discovered a polypeptide in red cells that we didn't expect to see. Interestingly, it was identical to a polypeptide in the kidney. So, on a great leap of faith, we decided to clone the complementary DNA (cDNA). This was in the early days before the genome was sequenced, so it was a lot of hard work. We obtained a cDNA encoding a 269–amino acid polypeptide. Identical transcripts were obtained from red cell and kidney libraries. The new protein was found to have six bilayer-spanning domains. The N-terminus of the protein resides within the cell, and then two interesting repeats appear, each corresponding to three bilayer-spanning domains. They are not a perfect sequence repeats but are genetically similar sequences. Most curiously, the two repeats appear to be oriented at 180° to each other. We looked at the DNA database in 1991. We found a number of similar sequences had been reported, but none of the proteins had a function that had been defined. Thus, we obtained no obvious clue to the function of our protein. The related sequences corresponded to a protein from the lens of eye from beef cattle, a protein from brain of *Drosophila* fruit flies, a protein that permits *Escherichia coli* to use glycerol as a carbon source, and a series of related proteins from various plant tissues. It was really the observation that red cells and kidney tubules are highly water permeable, and the existence of plant homologs, that caused us to pursue this further.

We established the water transport function of our protein in collaboration with our colleague Bill Guggino in the Physiology Department at Johns Hopkins. To do this, we injected the complementary RNA into *Xenopus laevis* oocytes. These amphibian eggs are about a millimeter in diameter and are known to be quite water impermeable (Figure 1). On the left is a controlled oocyte injected only with buffer alone and on the right is an oocyte injected with the complementary RNA for our new protein. After culture, the oocytes looked about the same. But when they were then dropped into distilled water, an amazing difference was observed. The controlled oocyte had failed to swell, the test oocyte had swollen and exploded. This produced much jubilation in the laboratory! Shown in Figure 1 is Gregory Preston, the Postdoctoral Fellow who did these studies. I took this photograph of Greg three years after the discovery, and he was still celebrating. So, I think that young scientists need to know that gratification is often delayed in science, and it is even permissible to cheer for yourself.

(*Received in original form October 19, 2005; accepted in final form December 6, 2005*)

Supported by grants from the National Heart, Lung, and Blood Institute, and a grant from the National Eye Institute.

Correspondence and requests for reprints should be submitted to Peter Agre, M.D., Duke University School of Medicine, DUMC 3701, Durham, NC 27710. E-mail: dr.agre@duke.edu

Proc Am Thorac Soc Vol 3. pp 5–13, 2006
DOI: 10.1513/pats.200510-109JH
Internet address: www.atsjournals.org

We spent a considerable amount of effort studying the structure of our new water channel protein. The internal repeats contain two loops B and E, which join the second and third, then the fifth and sixth bilayer-spanning domains and contain a degree of hydrophobicity. We thought that loops B and E may actually fold together and make a central aqueous pore. There is a special motif (Asn-Pro-Ala [NPA]) in each loop that overlaps in the center of the pore. The original hourglass model was just a pencil-and-paper sketch. But in fact it has been confirmed by high-resolution protein studies that we undertook with Professor Yoshinori Fujiyoshi from Kyoto, Japan, and Professor Andreas Engel from the Biocenter in Basel, Switzerland.

Together with these scientists, we solved the structure of the highly purified AQP1 protein from our lab. The reconstituted protein was 100% water permeable, indicating that the structure that we would deduce would be the biologically relevant structure. By a combination of cryo-electron microscopy and atomic force microscopy, a three-dimensional electron density map at 3.8-Å resolution was calculated, and models were built. The protein is tetromeric, but the functional unit is the monomer. A single aqueous pore passes down through the center of the protein. The protein fold has been further defined by X-ray photographic studies from Bob Stroud from the University of California, San Francisco, and Bing Jap from Lawrence Berkeley Laboratory. Molecular dynamic simulations were undertaken by deGroot and Grubmüller in Göttingen and Schulten and colleagues at the University of Illinois at Urbana-Champaign.

We now have a clear understanding of how the aquaporin proteins work. Aquaporins have a narrow pathway that is a very tight fit for water, the smallest biological molecule (Figure 2). Shown in Figure 2 is a space-filling representation of the single water molecule in the very center of the pore of the cross-section,

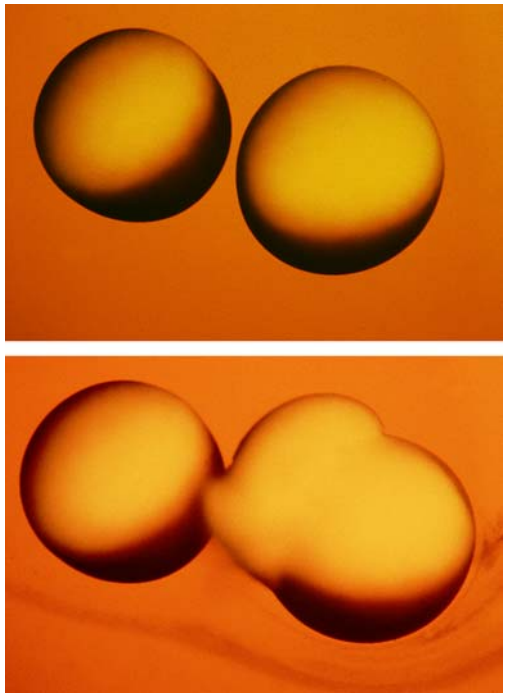

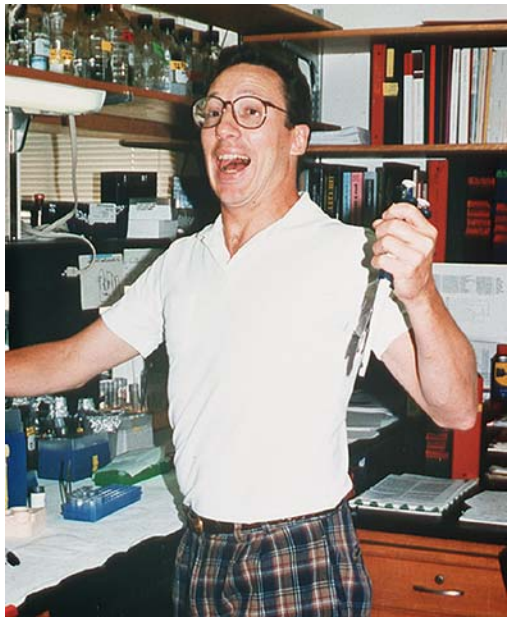

Figure 1. Discovery of aquaporin-1 (AQP1). Functional demonstration of water transport in *X. laevis oocytes*. *Top panel*: Control oocyte not expressing AQP1 (*left*) and test oocyte expressing AQP1 (*right*) 15 s after transfer to hypoosmotic culture medium. *Middle panel*: Same oocytes 3 min after transfer to hypoosmotic culture medium. The control oocyte failed to swell. The test oocyte swelled rapidly by osmosis and ruptured. Reprinted by permission from Preston GM, Carroll TP, Guggino WB, Agre P. Appearance of water channels in *Xenopus* oocytes expressing red cell CHIP28 protein. *Science* 1992;256:385–387. *Bottom panel*: Jubilation expressed by Postdoctoral Fellow Gregory Preston 3 years after original report.

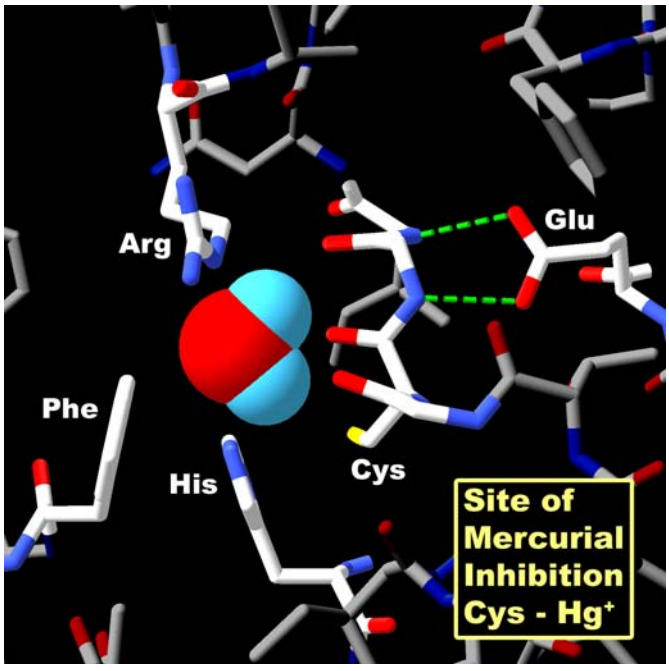

Figure 2. Structure of AQP1–Hg^{++} inhibitory site. Space-filling representation of a single water molecule in the narrowest point in the pore. Surrounding residues arginine-195 (Arg) and histidine-180 (His) provide positive charges that repel protons. Cysteine-189 (Cys) is the site of Hg^{++} inhibition. Phenylalanine-56 (Phe) and glutamic acid-142 (Glu) are other important residues in the pore region. Reprinted by permission from Kozono D, Yasui M, King LS, Agre P. Aquaporin water channels: atomic structure molecular dynamics meet clinical medicine. *J Clin Invest* 2002;109:1395–1399.

and you can see that the adjacent charged residues, arginine and histidine, are very close. One can see here that there is a perfectly conserved residue, a cysteine, which is the site of mercurial inhibition. Now, how did this water pass through the membrane, but fail to carry protons? My father was a chemistry professor back in Minnesota, and he liked to tell his first-year students about the chemistry of water—H_2O. Because it is 18 Da in mass, the molecule would be predicted to be a gas, which of course water is in the atmosphere. But in solution, the hydrogen bonds between water molecules cause water to be a liquid. In bulk solution, the water molecules are close together and hydrogen bonding occurs. This allows free movement of protons hopping between the molecules. In the extracellular vestibule of the hourglass and in the intracellular vestibule, water exists in bulk solution (Figure 3). But the center of the aquaporin has a 20-Å trim span where water transits the pore in single file. The narrowest diameter of the pores is 2.8 Å—just big enough for a single water molecule. A fixed positive charge on the adjacent arginine side chain will repel protons. The water molecules then are spaced within the pore at intervals so that hydrogen bonding cannot occur between them. A second barrier exists in the center of the pore, where an isolated water molecule will transiently form hydrogen bonds to the side chains of two highly conserved asparagines residues. This provides a very interesting mechanism—one that allows water to move with no resistance.

We and others sought by homology cloning to identify other members of the aquaporin protein family. A gene pileup represents a partial listing of human aquaporins (Figure 4). We now know of 12 human sequences that are closely related to AQP1. They are classed into two subsets: those permeated by water alone, the classical aquaporins, and those permeated by water plus glycerol, the aquaglyceroporins. Knowing the biophysical functions of the proteins and the sites where they are expressed permits us to predict their physiologic and pathophysiologic functions. I will briefly discuss some of each subset. AQP1 in the kidney is responsible for the countercurrent concentrating mechanism in the proximal tubules. AQP2 is the vasopressin-regulated water channel in the collecting duct. Mutations in the gene encoding AQP1 cause mild nephrogenic diabetes insipidus, but mutations in the gene encoding AQP2 are much more severe. AQP4 is expressed in brain, and is involved in both the pathogenesis and the recovery from brain edema. AQP0 is expressed in lens, and mutations in this protein cause cataracts. The aquaglyceroporin AQP7 is expressed in fat tissue where it is responsible for glycerol release during fasting and starvation, while AQP9 in liver permits glycerol uptake by liver for gluconeogenesis.

To define the physiologic functions of AQP1, we collaborated with Søren Nielsen from the University of Aarhus in Denmark who is a world-class microscopist. Søren localized the AQP1 in lung and other tissues as well, but lung is the topic of the talk today. AQP1 is present in the capillary endothelium in a peribronchiolar distribution. In the alveolar section, a lower degree of specific staining is visible (Figure 5). Immunogold electromicroscopy of a single capillary endothelial cell from human lung exhibits immunogold labeling of both the lumenal membrane and the ablumenal membrane of the capillary (Figure 6). Studies by our colleague Landon King in the Division of Respiratory and Critical Care Medicine at Johns Hopkins demonstrated that the level of AQP1 expression in lung microvasculature is not constant. The amount of AQP1 rises dramatically in lung at the time of birth. In addition, AQP1 expression is exquisitely sensitive to corticosteroids—about an eightfold increase in expression in adult rat lung (Figure 7, *left panel*). Like many others, I suffer from a mild form of asthma; I use a corticosteroid inhaler, and the beneficial effects may be partly explained by the induction of AQP1 expression.

AQP1 protein expression can be induced, but expression levels can also be reduced, because the protein is degraded by the ubiquitin pathway. Here I should add that my talk is going to lead up to the one by Aaron Ciechanover, discoverer of the ubiquitin pathway (*see* page 21). In another study, Landon King looked at the degradation of AQP1 by the ubiquitin proteosome in cultured fibroblasts (Figure 7, *right panel*). Fibroblasts normally only express very low levels of AQP1 when cultured in isotonic medium. Immunoprecipitations analyzed by antiubiquitin immunoblotting show that the AQP1 is polyubiquitinated—a low level of AQP1 is expressed and rapidly ubiquitinated targeting the protein for degradation. When fibroblasts are grown in culture medium made hypertonic by the addition of 200 mOsm sorbitol, the protein accumulated in abundance. Immunoprecipitations analyzed by antiubiquitin immunoblotting show that when fibroblasts are grown in hypertonic media, AQP1 is not ubiquitinated, and the level of protein rises dramatically. This provides an efficient mechanism for effectively accumulating AQP1 protein when it is needed and rapidly reducing AQP1 protein when no longer needed by the cell.

The lung is complicated, and Søren Nielsen and Landon King have defined the presence of multiple aquaporins at different levels of the respiratory tree (Figure 8). As described, AQP1 is present in capillaries and fibroblasts below the basement membrane. A different expression pattern is seen in the surface epithelium that lies above the basement membrane. Surface columnar cells contain AQP4 along the basolateral membranes. The adjacent goblet cells apparently do not contain aquaporins. The basal cells that reside along the basement membrane do not reach the surface and express high levels of AQP3. Thus, a clear distinction exists at the sites where AQP1, AQP3, and AQP4 are expressed. Still more complexity is found in the submucosal glands where AQP5 is expressed.

How does one distinguish the importance of multiple aquaporin proteins that exist alongside each other in the complex airway epithelia? The level of expression is tightly regulated during fetal development. AQP1 and AQP3 are expressed before birth, but AQP4 is only expressed after birth. So here is an example of where clinical medicine provides basic scientific insight. Mice with gene knockouts have been prepared and have provided important insight. But as physicians, we are really interested in the human biology.

The structural gene for AQP1 is colocalized with a specific blood antigen on human chromosome 7. As a hematologist, I am interested in blood group antigens. Although there are hundreds of different antigens, they comprise about 25 families—each family being a genetic locus. As it turns out, the Colton blood antigen (Co) is a simple polymorphism on the surface of the AQP1 protein. Most of us have the same Co blood types, so they are usually not important clinically. Nevertheless, our colleagues at the International Blood Group Referencing Laboratory in Bristol, England, have only identified a handful of individuals lacking Co. So of course these are the very people that we became interested in. The Co-null individuals we were able to study were all women who apparently became sensitized during pregnancy. We determined that each was homozygous for different disrupting mutations in the gene encoding AQP1—a frameshift, an exon deletion, or a structurally important missense mutation—and were AQP1-null. Our Johns Hopkins colleague Landon King studied two unrelated AQP1-null individuals. A longstanding and distinguished member of the ATS, Landon was an ideal scientist to evaluate AQP1 in lung. The AQP1-null individuals have circulating anti-Co antibodies and are unable to tolerate a blood transfusion from other blood donors.

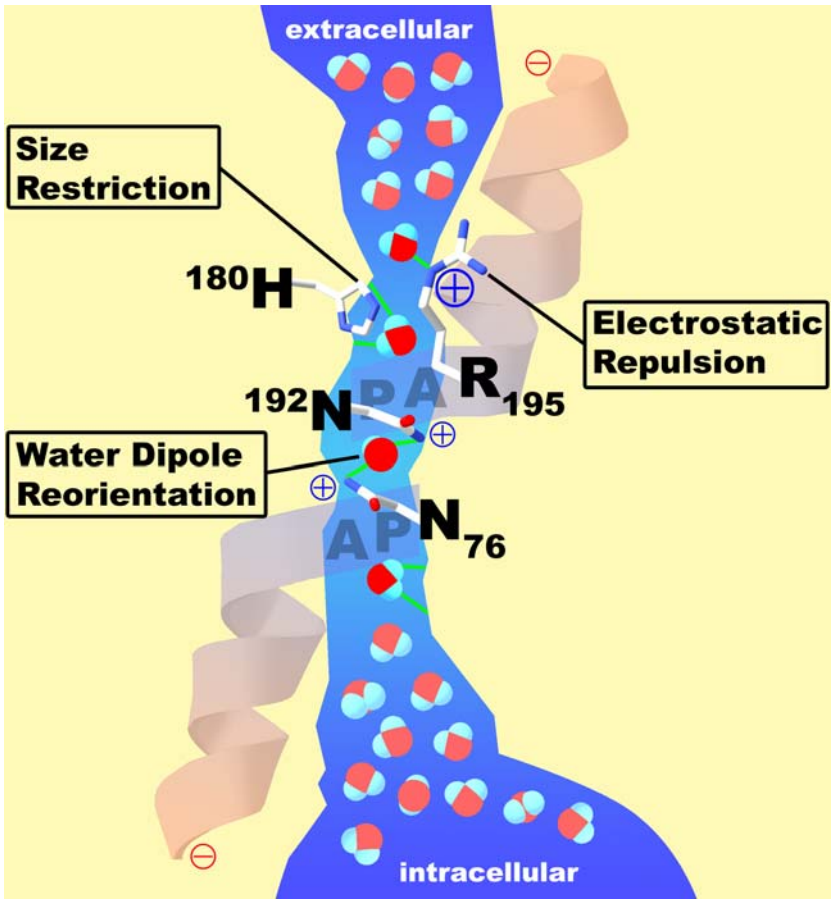

Figure 3. Functional schematic for water passage through AQP1. The extracellular vestibule and the intracellular vestibule of the channel contain water in bulk solution. They are connected by a 20-Å span where water molecules pass in single file. Barriers to the passage of protons are visible. Arginine-195 (R195) and histidine-180 (H180) provide fixed positive charges to repel proton passage. A single water molecule forms hydrogen bonds with the side chains of highly conserved asparagines-76 and -192 (N76 and N192). Partial positive charges are provided by the orientation of the two α helices that enter but do not entirely span the bilayer. Reprinted by permission from Kozono D, Yasui M, King LS, Agre P. Aquaporin water channels: atomic structure molecular dynamics meet clinical medicine. *J Clin Invest* 2002;109:1395–1399.

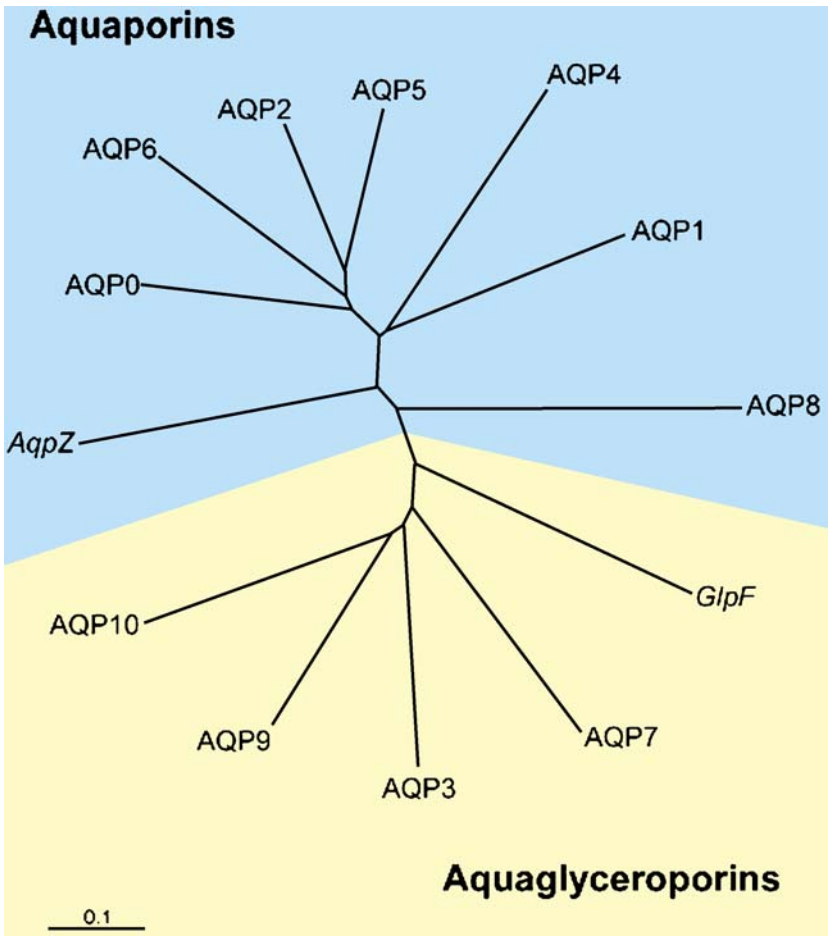

Figure 4. Human aquaporin repertoire. Two subsets of members exist: those permeated only by water (aquaporins) and those permeated by water plus glycerol (aquaglyceroporins). Included are the two members from *Escherichia coli*: AqpZ, a water channel, and GlpF, a glycerol transporter. Reprinted by permission from Kozono D, Yasui M, King LS, Agre P. Aquaporin water channels: atomic structure molecular dynamics meet clinical medicine. *J Clin Invest* 2002;109:1395–1399.

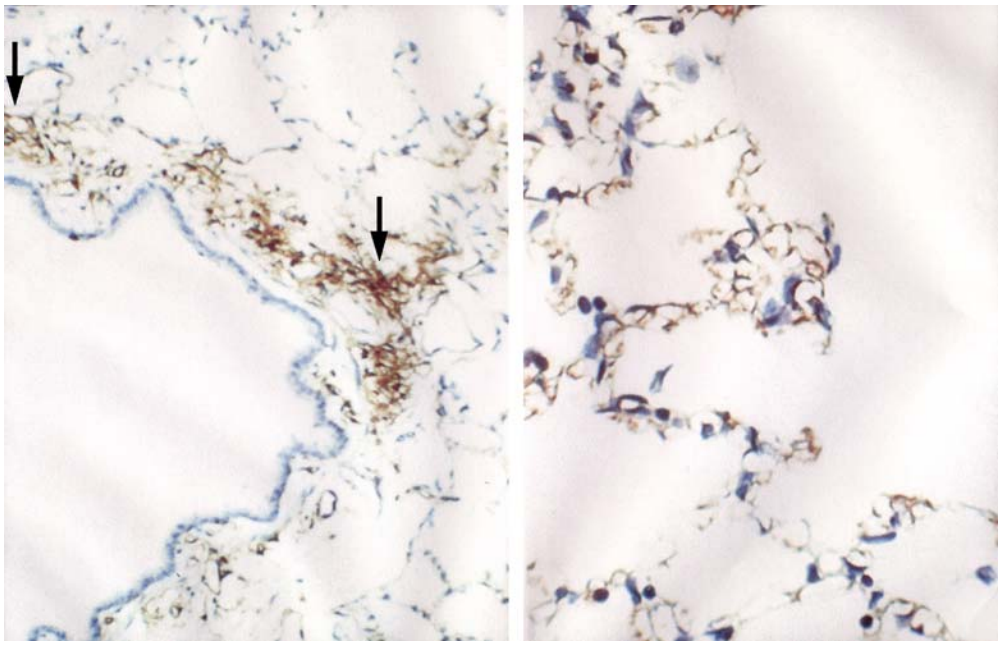

Figure 5. AQP1 in rat lung capillary endothelium. *Left panel*: Immunoperoxidase staining reveals AQP1 in capillary endothelium (*arrows*) in peribronchiolar distribution. *Right panel*: Immunoperoxidase staining reveals AQP1 in capillary endothelium in alveolar distribution. Reprinted by permission from Nielsen S, Smith BL, Christensen EI, Agre P. Distribution of the aquaporin CHIP in secretory and resorptive epithelia and capillary endothelia. *Proc Natl Acad Sci* 1993;90: 7275–7279.

Nevertheless, the AQP1-null individuals look and feel well. But clinical medicine provides us with a very interesting and powerful approach to identifying the importance of proteins. Presumably, many of us bear mutations in different genes. While these mutations usually do not cause symptoms, if we're properly stressed, they can provoke a disease phenotype.

Landon King, in collaboration with Robert Brown at Johns Hopkins, used high-resolution computed tomography scans of the lung to evaluate lung capillary water permeability of these individuals before and after intravenous infusion of saline. Shown in Figure 9 are images from normal individuals: a 2-mm bronchiole and an adjacent venule at baseline and the same structures after infusion of 3 L of physiologic saline. It is obvious that the venule has become distended after intravenous fluid caused engorgement of the blood microvasculature. Similar increases are found in all normal individuals and all of the AQP1-null individuals. After infusion of saline, the wall thickness of the bronchioles in all normal individuals has increased due to water released from the blood vessels into the surrounding soft tissues. Thus, the bronchiolar wall thickness has increased as water collects in the perivascular soft tissues, forming incipient pulmonary edema. Surprisingly, the AQP1-null individuals had no such release of fluid to the surrounding soft tissues. Their bronchioles remained unchanged throughout the study—strong evidence that they have clear and measurable decrease in the vascular water permeability. At this point, we can only speculate about the clinical significance of this finding. With the first breath of life, the infant's lung absorbs amniotic fluid through the airway epithelium, and this is taken into the surrounding blood vessels. Thus, AQP1 may be important in perinatal fluid absorption by lung. If this is a reason for the low prevalence of the AQP1-null state, then presumably those who survive are somehow compensating for the lack of AQP1 in the microvasculature.

Now, I will talk about another aquaporin from the lungs: AQP5 is expressed in secretory glands, including airway submucosal glands, lacrimal glands, salivary glands, and sweat glands. AQP5 is expressed in the apical membrane of the secretory glands (Figure 10). The apical membrane where AQP5 resides is the last membrane water passes through during the secretion of airway fluids, tears, saliva, and sweat. Evidence suggests that this is important in clinical medicine. One study undertaken in collaboration with Chris Delporte in Brussels and a second study undertaken in collaboration with Kazuo Tsubota in Tokyo analyzed biopsies from a small number of patients with Sjögren's syndrome. This well-recognized disorder leads to dry eye and dry mouth problems, and pulmonary disorders as well. While

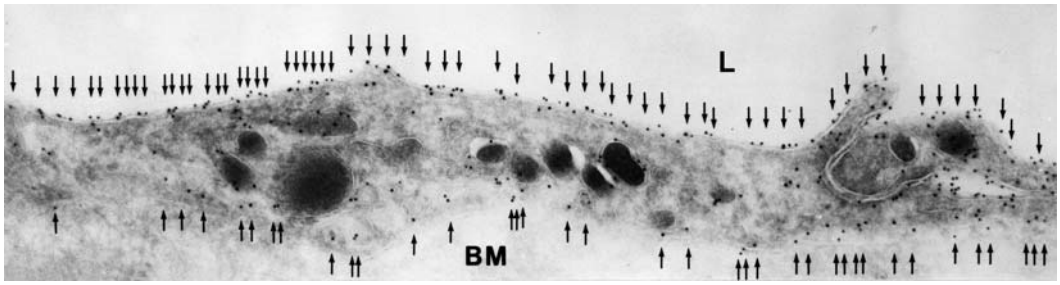

Figure 6. AQP1 in human lung capillary endothelium. Immunogold electron microscopic analysis reveals labeling of plasma membranes on lumenal surface (*top)* and ablumenal surface (*bottom*). Reprinted by permission from King LS, Nielsen S, Agre P, Brown RH. Decreased pulmonary vascular permeability in aquaporin-1-null humans. *Proc Natl Acad Sci* 2002;99: 1059–1063.

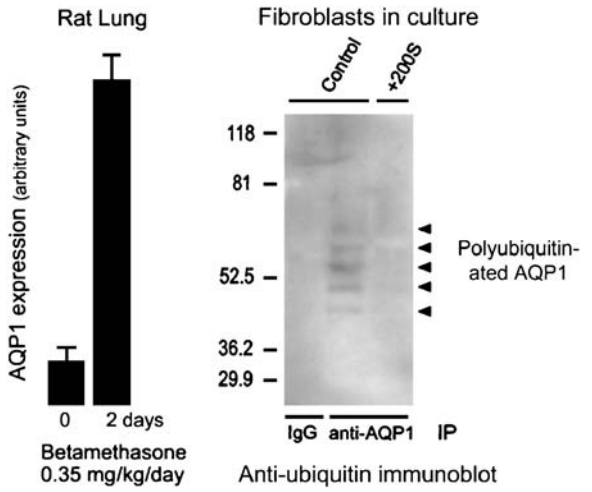

Figure 7. Dynamics of AQP1 expression. *Left panel*: Expression of AQP1 in rat lung is induced by corticosteroid exposure for 2 d. Reprinted by permission from King LS, Nielsen S, Agre P. Aquaporin-1 water channel protein in lung: ontogeny, steroid-induced expression, and distribution in rat. *J Clin Invest* 1996;97:2183–2191. *Right panel*: Level of AQP1 expression in cultured fibroblasts induced by hypertonic shock is regulated by degradation through the ubiquitin–proteosome pathway. Controls (*left lane* and *center lane*) denote fibroblasts grown in isotonic culture media producing extremely low levels of AQP1 accumulation. +200S denotes fibroblasts grown in culture medium made hypertonic by addition of 200 mOsm sorbitol. Anti-AQP1 immunoprecipitation (IP) was followed by antiubiquitin immunoblot. The *left lane* shows no signal in the control lacking immunoprecipitation control. The *center lane* shows polyubiquitination of AQP1 (ladder of reactive bands) in fibroblasts grown in isotonic culture media, thereby keeping AQP1 expression levels low. The *right lane* shows no polyubiquitination of AQP1 in fibroblasts grown in hypertonic culture medium, allowing AQP1 expression levels to rise to high levels. Reprinted by permission from Leitch V, Agre P, King LS. Altered ubiquitination and stability of aquaporin-1 in hypertonic stress. *Proc Natl Acad Sci* 2001;98:2894–2898.

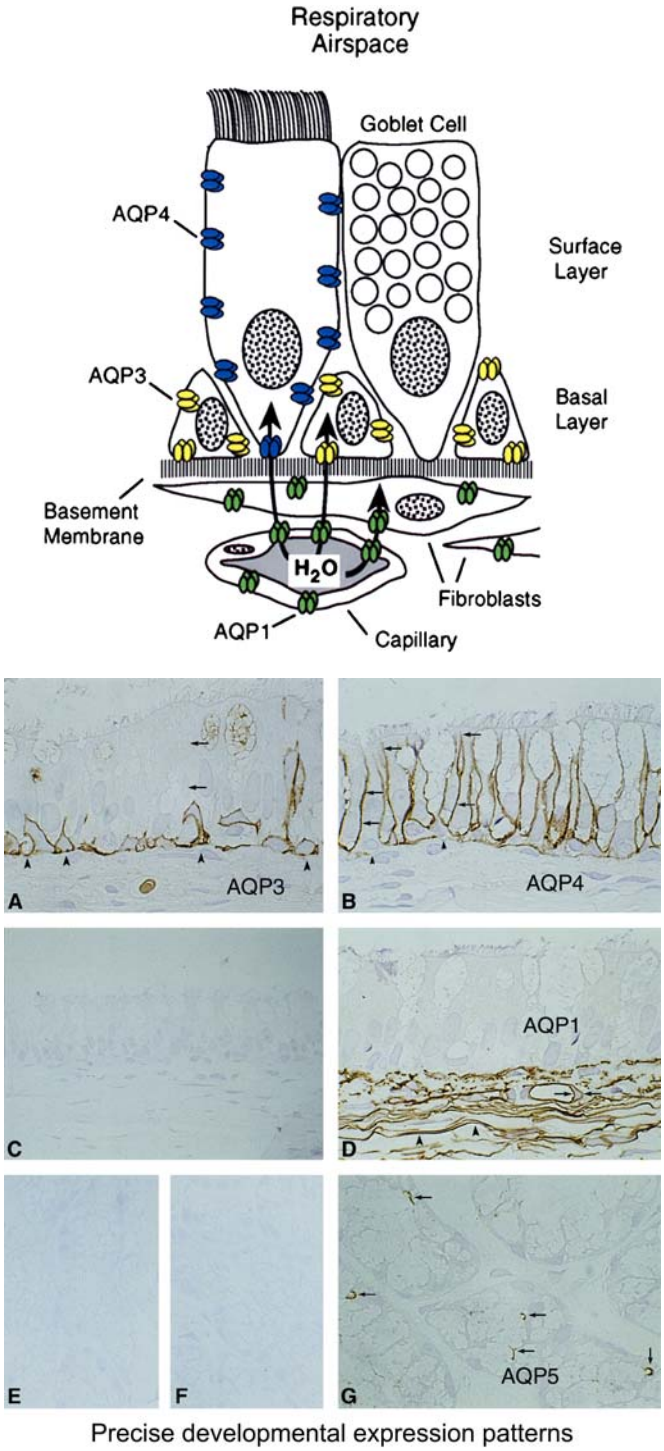

Figure 8. Aquaporins in respiratory epithelia. *Upper panel*: Schematic demonstrating absence of aquaporin expression in goblet cells, AQP4 in surface columnar cells, AQP3 in basal cells, and AQP1 in underlying fibroblasts and capillaries. *Lower panels*: Immunoperoxidase, brown staining, reveals aquaporins in rat tissue sections corresponding to nasopharyngeal surface epithelium. (*A*) AQP3, (*B*) AQP4, (*C*) AQP5 (no staining). and (*D*) AQP1. Immunoperoxidase, brown staining, reveals aquaporins in rat tissue sections corresponding to subepithelial glands. (*E*) AQP3 (no staining), (*F*) control (no staining,) and (*G*) AQP5 (staining of apical surface). Reprinted by permission from Nielsen S, King LS, Christensen BM, Agre P. Aquaporins in complex tissues. II. Subcellular distribution in respiratory and glandular tissues of rat. *Am J Physiol Cell Physiol* 1997; 273:C1549–C1561.

Sjögren's syndrome is known to be an autoimmune problem, loss of glandular function often occurs in glandular elements where infiltration of lymphocytes is not seen. Normal biopsies have intense anti-AQP5 staining at the apical surface (Figure 11, *left panel*). In contrast, diffuse presence of AQP5 protein is notable throughout the glandular epithelium (Figure 11, *center panel*). This indicates that a mistake in trafficking of AQP5 protein has occurred, presumably as a secondary defect. An independent study of a larger number of Sjögren's syndrome biopsies was undertaken by Roland Jonsson, from the University of Bergen in Norway, and his collaborators. Interestingly, these investigators found normal AQP5 distribution, but they determined that AQP1 expression was reduced in the surrounding myoepithelial cells surrounding the glandular acini. So while there appears to be heterogeneity, all three groups found some aquaporin defects in this important clinical disorder, Sjögren's syndrome, and we can as yet only speculate what is happening in submucosal glands of lung.

Another important role of AQP5 is in sweat glands. In collaboration with Lene Nejsum and Søren Nielsen, analysis of sweat glands was undertaken comparing normal mice with AQP5 gene knockout mice engineered by Anil Menon and Carissa Krane from the University of Cincinnati. Although both mice have normal-appearing sweat glands, the AQP5-null mice exhibit diminished function of sweat glands after pharmacologic stimula-

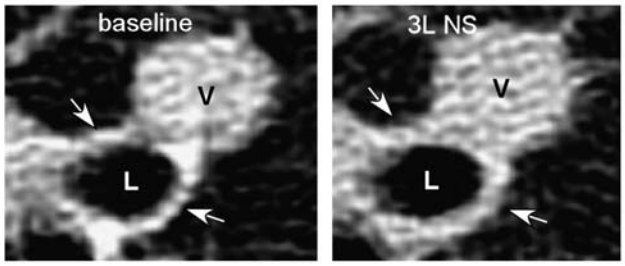

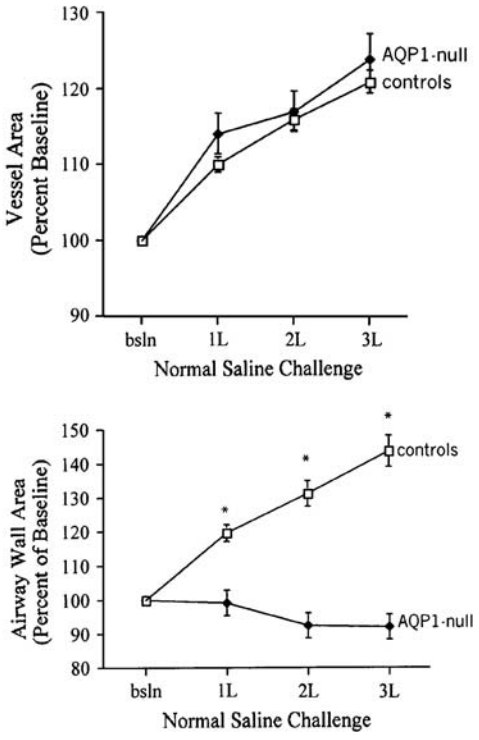

Figure 9. AQP1-null humans—pulmonary capillary defect. *Left panels*: High-resolution computed tomography scan of lung before (*left*) and after (*right*) infusion of 3 L of physiologic saline. The lumen of a 2-mm bronchiole is denoted (*L*) as well as an adjacent venule (*V*). After infusion of saline, the venule becomes engorged and the wall of the bronchiole becomes thickened due to accumulation of fluid (*see arrows*). *Upper right panel*: This was reproduced in multiple normal individuals. *Lower right panel*: When AQP1-null individuals were investigated, they did not accumulate fluid surrounding the bronchiole, since the vascular water permeability was reduced *$p<0.001$ between groups. Reprinted by permission from King LS, Nielsen S, Agre P, Brown RH. Decreased pulmonary vascular permeability in aquaporin-1-null humans. *Proc Natl Acad Sci* 2002;99:1059–1063.

tion. We do not yet have direct evidence for what is happening in airway submucosal glands; it is our belief an important function of AQP5 will be identified.

Another place where AQP5 is expressed in lung is in the type 1 pneumocytes in the alveoli. A simple model of the alveolar level of lung is shown (Figure 12, *upper panel*). The type 2 cells, where a number of transport functions are known to occur, lack AQP5, but the flattened type 1 cells contain an abundance of AQP5. Immunogold decoration reveals an abundance of AQP5 in the apical membranes but not in the basolateral membranes (Figure 12, *lower panel*). Leland Dobbs at the University of California in San Francisco has undertaken a classic study that demonstrated that these type 1 pneumocytes have the highest water transport capacity of any cell type in the body. While the physiologic significance is still uncertain, I would like to leave this challenge to the young scientists here. In contrast to kidney and eye, for which advanced understanding of the role of aquaporins has emerged, I think the importance of aquaporins in airways is still in need of a lot of research.

So in closing, I will talk about a completely irrelevant system in terms of human disease, but an interesting illustration of the ubiquity of the aquaporins. We now know that aquaporins are expressed in all life forms. *Arabidopsis thaliana* is a small mustard plant that is often the subject of investigation by plant physiologists. An interesting study executed by Ralf Kaldenhoff in Germany showed that parental strains of *A. thaliana* need only a slender group of rootlets to support the necessary water uptake of the plant. Kaldenhoff then engineered a genetically modified *A. thaliana* in which rootlet expression of the Pip1b group of aquaporins is only 20% of the normal level. While the plants looked fine from the surface up, the genetically modified plant has compensated for the reduced rootlet aquaporin expression by sending out many more rootlets. Plants are known to express dozens of aquaporins, and their tissue distribution is well preserved. Microorganisms also contain aquaporins, and we hope that some of these may prove to be useful targets for new antibiotic development.

Finally, to summarize my lecture, I talked about aquaporins and how they are selectively permeated by water but not acid. Certain homologs are permeated by other substrates, such as glycerol. The structural model explains the functions beautifully, and AQP1 is regarded as the first atomic structure of a human channel protein. Aquaporins have been implicated in a number of clinical disorders, but the roles of aquaporins in respiratory diseases remain poorly defined. It is easy to imagine what lung aquaporins might be doing in terms of osmotic water movements—freshwater drownings, for example. But how do lung aquaporins participate in asthma, cystic fibrosis, and wound healing, or in response to infection? I think these issues are quite relevant to the mission of the ATS, and I sincerely hope that some of the young scientists attending this meeting will take up this challenge.

Now, let me spend just a moment to tell you what it is like to win a Nobel Prize, since people often ask me. Well, it is a lot of fun, but it starts out a little puzzling. The phone rang in my bedroom at 5:30 in the morning on October 8, 2003, and a very distinguished Swedish gentleman notified me that I would share the Nobel Prize in chemistry. I was obviously delighted to hear the message, but my second thought was "chemistry, what in hell do I know about chemistry?" Our next speaker knows a lot about chemistry, since Aaron Ciechanover is a real biochemist. When I came to work a few hours after the phone call, I noticed there was a big party underway in my laboratory, organized by the young people in our group. Several ATS members were in the thick of it, including Landon and other members of his team, Virginia, Ramana, and Kelly, and were celebrating enthusiastically. Our university president even came over to see me—I had no idea that we were such good friends! My telephone voicemail was filled with requests for interviews, and then there was the voice of a very dear colleague from Norway. And I will never

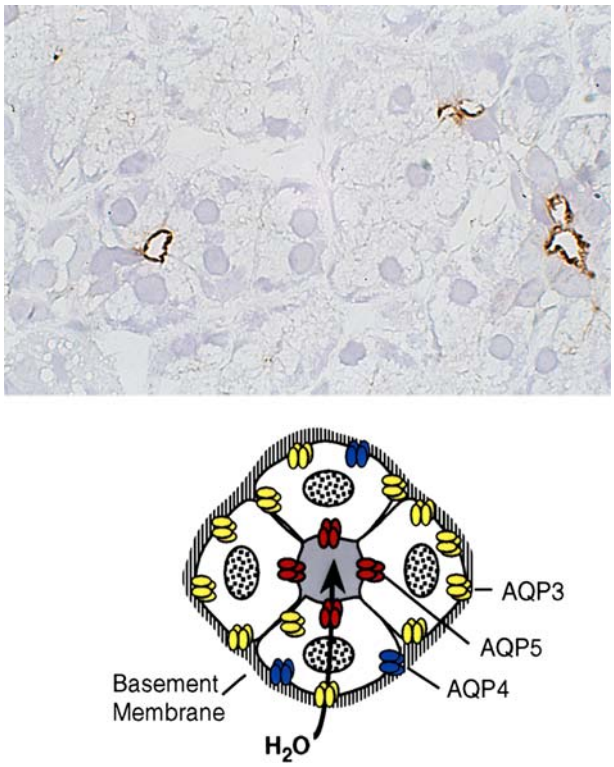

Figure 10. AQP5 in secretory glands. Drawings of secretory glands reveal AQP5, colored red, at the apical membrane (*lower panel*). The immunohistochemically stained tissue section of rat salivary gland reveals AQP5, stained brown, at the apical surface of three acini but not basolateral membranes (*upper panel*). Reprinted by permission from Nielsen S, King LS, Christensen BM, Agre P. Aquaporins in complex tissues. II. Subcellular distribution in respiratory and glandular tissues of rat. *Am J Physiol Cell Physiol* 1997;273:C1549–C1561.

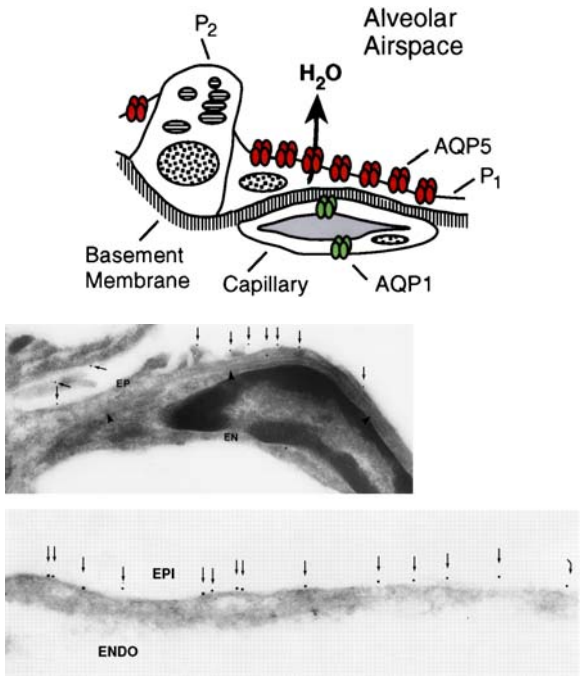

Figure 12. AQP5 in alveolar type 1 pneumocytes. *Upper panel*: Drawing of alveolar space reveals AQP5, colored red, in apical membrane of type 1 pneumocytes (P_1) but not type 2 pneumocytes (P_2). *Middle and lower panels*: Immunogold labeling of AQP5 at apical membranes denoted with *arrows*. ENDO = endothelium; EPI = epithelium. Reprinted by permission from Nielsen S, King LS, Christensen BM, Agre P. Aquaporins in complex tissues. II. Subcellular distribution in respiratory and glandular tissues of rat. *Am J Physiol Cell Physiol* 1997;273:C1549–C1561 (*upper* and *middle panels*); King LS, Nielsen S, Agre P. Respiratory aquaporins in lung inflammation: the night is young. *Am J Respir Cell Mol Biol* 2000;22:8–10 (*lower panel*).

forget his voice; he said, "Peter, Peter, we just heard the news—it's unbelievable." So that shows the confidence that your colleagues may have for you. But then the voice came back on and said, "No, no, it's very believable—it's wonderful." And if the day wasn't crazy enough, while driving home that evening, the large sign in front of the discount liquor store at our neighborhood shopping center read, "Congrats Dr. Agre" in large letters, indicating that I already had become a local celebrity. And I'd just like to point out the implication that I am their best customer is really a great exaggeration. When I got home, our youngest daughter was home from high school, and she's a real shy kid. I told her I hoped that others would not bother her at school

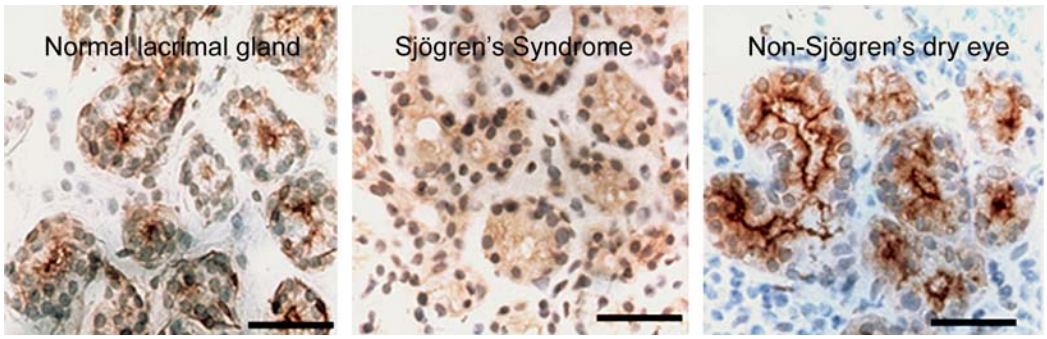

Figure 11. AQP5 in lacrimal glands—anti-AQP5 immunohistochemical staining of normal versus Sjögren's syndrome biopsies. Paraffin sections of human biopsies show AQP5, brown staining, in the apical membrane of normal (*left panel*) and non-Sjögren's dry eye (*right panel*). *Center panel*: The biopsy from a patient with Sjögren's syndrome reveals diffuse staining over the cell body indicating that a mistake in membrane trafficking had occurred. Studies by other investigators (Beroukas and colleagues) did not reveal abnormal AQP5 distribution but demonstrated AQP1 is reduced in myoepithelium (not shown). Reprinted by permission from Tsubota K, Hirai S, King LS, Agre P, Ishida N. Defective cellular trafficking of lacrimal gland aquaporin-5 is Sjögren's syndrome. *Lancet* 2001;357:688–689.

about this, and she said the most amazing thing that a teenager could tell her dad, “No, Daddy, my friends tell me this is so cool, but you should know that really famous people are on Simpsons and you’re not.”

So, with that, let me thank you again for the invitation to be here at the ATS Centennial—THANK YOU!

***Conflict of Interest Statement*:** P.A. does not have a financial relationship with a commercial entity that has an interest in the subject of this manuscript.

See potassium run

Christopher Miller

Nearly all cells have membranes spanned by potassium-conducting channel proteins, without which your nerves (and much else) simply wouldn't work. Ion permeation through these channels can now be seen in dazzling detail.

Scientific discovery has its breakthroughs, and breakthroughs their aftermaths. Three years ago, Roderick MacKinnon's group at Rockefeller University in New York achieved a stunning advance in molecular neurobiology with the first atomic-resolution picture of a potassium (K^+) channel[1]. Three papers in this issue[2–4] now give us a mechanistic and dynamic view of how these pore proteins work.

Potassium channels are important membrane-spanning proteins that directly catalyse the ionic movements required to generate and shape electrical signals in neurons (and also in many other cells not so well endowed with brain-associated pizzazz). The original structure[1], though a bit fuzzy at 3.2 Å resolution, evoked gasps as it revealed the molecular design of these pores. It gave hope for an eventual understanding of the perplexing functional hallmark of K^+ channels — the combination of high selectivity and rapid throughput that allows K^+ to pass at such high rates that the protein seems to present no barrier at all, while simultaneously acting as a concrete wall to the smaller Na^+ ion.

The structure[1] sketched out the molecular basis of this specificity: a narrow 'selectivity filter' in the shape of an oxygen-lined electronegative tunnel in which dehydrated K^+ (but not Na^+) fits precisely. This structure rationalized why a K^+ ion is so willing to leave its thermodynamically comfortable home in aqueous solution to enter the pore in a largely dehydrated form; the channel interior mimics the embrace of the water molecules in the inner hydration shell surrounding the ion in solution.

And now, the aftermath. MacKinnon's group[2,3] (pages 37 and 43) presents an improved structure of the K^+ channel, while Bernèche and Roux[4] (page 73) carry out computer simulations of this same channel protein; together the results provide a deep understanding of how ions diffuse through this pore so rapidly. The new X-ray crystallographic structures, at a sharp 2 Å resolution, are dazzling. They offer three fundamental insights into the physical chemistry of ion conduction in biology: they show how ions are coordinated in the selectivity filter; they reveal the nature of K^+ ions in transit between the channel and the aqueous solvent; and they indicate the character of water in the cation's inner hydration shell.

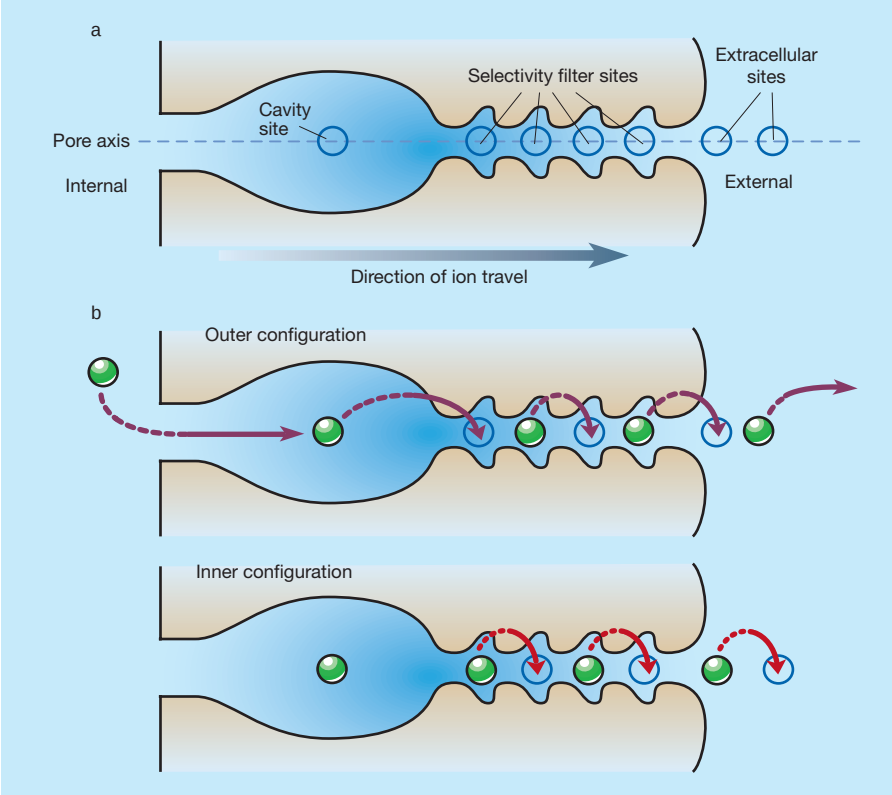

Figure 1 **Permeation of K^+ ions through the pore of a K^+ channel, as surmised from the new results[2–4] discussed here.** a, **There are seven main sites for ions along the pore axis: one in the pore cavity, four in the selectivity filter and two just beyond the external end of the pore. The cavity site is fully occupied, but (as indicated in** b**) only half of the remaining six are occupied at any one time.** b, **The two main ion configurations, known as outer and inner, that are postulated to exist within the pore. Purple arrows indicate ion shifts that are linked directly to concerted ion entry into and exit from the pore. Red arrows represent shifts within the pore without ion entry and exit. As shown here, then, ion passage through the selectivity filter and extracellular sites occurs in bucket-brigade fashion.**

According to the familiar cautionary riff, X-ray crystallography is a snapshot-based technique impoverished in dynamic information about protein function. But these new pictures let the viewer imagine K^+ ions actually traversing the pore, because they catch the ions at several stages of movement. This is an unusual situation, unknown, for example, in crystallographic enzymology, which seeks to freeze the substrate at different stages of chemical transformation, each requiring a separate crystal structure. With K^+ channels, a single image makes these multiple stages visible all at once because, in contrast to enzymes, channels process several substrate ions simultaneously in bucket-brigade fashion[5,6]. Potassium ions are now seen in seven distinct sites along the pore-axis (Fig. 1a). Four of these reside in the narrow selectivity filter, and one in the wider hydrated cavity, as described earlier[1,7]. By solving structures at varying ion concentrations, MacKinnon and colleagues argue that the four selectivity-filter sites are not all occupied simultaneously; rather, a pair of K^+ ions separated by a single water molecule shifts in a concerted fashion between two configurations within the filter — inner and outer — occupying each about half the time (Fig. 1b).

This ion-shifting between two pairs of positions, presumably on the conduction timescale of 10–100 nanoseconds, is at the heart of the permeation mechanism emerg-

ing from this work. As any long-distance cyclist knows, you make better time on level ground than in terrain with hills or valleys. It's the same for channel-dwelling K^+ ions, which permeate so rapidly because, as shown here by ion-occupancy measurements, the inner and outer ion configurations are precisely balanced in free energy, perfectly designed to eliminate barriers to high throughput. This point is buttressed by experiments with Rb^+ — a slightly larger, non-biological K^+ analogue indifferent to the demands of evolution — for which the two configurations are energetically out of balance; the resulting hilly landscape deduced from the X-ray data crisply explains the slower conduction of Rb^+ (refs 3, 8).

Two big surprises leap out of the results, and both enrich our comprehension of what life is like for ions diffusing through the channel. First, K^+ shows up at two additional on-axis positions just beyond the extracellular end of the pore, positions partially occupied by an ion shifting between the two. This ion is mainly in contact with aqueous solvent, so it is astonishing that it is localized enough to be visible in the electron-density maps used to pinpoint features by X-ray crystallography; strong electrostatic focusing by the channel surface is the likely explanation. Most dramatically, in the position closest to the pore entrance a K^+ ion is caught *in flagrante*, coordinated in front by four protein carbonyl groups reaching outwards, and behind by solvent; this must represent the long-postulated 'dehydration transition state' in which the ion sheds its water while entering the pore[9]. It is now seen not to be a high-energy transition-state at all, but rather a true intermediate, an integral part of the flat landscape.

Remarkably, in an independent computer simulation[4], Bernèche and Roux anticipated that a K^+ ion would be localized in solvent, right at the two sites where it is actually seen in the X-ray work. This successful prediction in advance of the facts — a rarity in computational biochemistry — enhances the confidence of sceptical experimentalists in the methods and parameters used in this theoretical work. This tends to fortify an additional conclusion emerging from the work — that not only are the K^+-binding configurations energetically similar, but so are the transitions between them. This means that the entire conduction process is energetically barrierless. So, overall, K^+ permeation looks rather like the concerted action of those steel pendulum toys known as Newton's balls. An ion entering the pore on the left expels an ion on the right into solution, while the four ions within and just outside the pore all shift one position to the right (Fig. 1b); if this occurs on energetically level ground, the process will be rapid.

The second surprise in the X-ray results is a structure that has often been imagined but never before glimpsed: the complete inner hydration shell of an aqueous cation. The channel's central cavity has room for about 50 water molecules, along with the single hydrated K^+ ion suspended there. Here, eight of these waters are individually visible, with their oxygens packed directly against the K^+ ion at the corners of a twisted cube. This inner-shell geometry closely matches the arrangement of the K^+-coordinating oxygens in the selectivity filter, and the authors wonder whether it might also mirror K^+ hydration in bulk liquid water. If so, they intimate, perhaps the four-fold architecture of K^+ channels evolved around the structure of hydrated K^+ to create an energetically welcoming home — the ultimate flat landscape — for ions forced to strip on their swift journey from one side of the membrane to the other. ■

Christopher Miller is in the Department of Biochemistry, Howard Hughes Medical Institute, Brandeis University, Waltham, Massachusetts 02468, USA.
e-mail: cmiller@brandeis.edu

1. Doyle, D. A. *et al. Science* **280,** 69–76 (1998).
2. Morais-Cabral, J. H., Zhou, Y. & MacKinnon, R. *Nature* **414,** 37–42 (2001).
3. Zhou, Y., Morais-Cabral, J. H., Kaufman, A. & MacKinnon, R. *Nature* **414,** 43–48 (2001).
4. Bernèche, S. & Roux, B. *Nature* **414,** 73–77 (2001).
5. Hodgkin, A. L. & Keynes, R. D. *J. Physiol. (Lond.)* **128,** 61–88 (1955).
6. Neyton, J. & Miller, C. *J. Gen. Physiol.* **92,** 569–586 (1988).
7. Jiang, Y. & MacKinnon, R. *J. Gen. Physiol.* **115,** 269–272 (2000).
8. LeMasurier, M., Heginbotham, L. & Miller, C. *J. Gen. Physiol.* **118,** 303–314 (2001).
9. Hille, B. *Ion Channels of Excitable Membranes* (Sinauer, Sunderland, MA, 2001).

Quantum optics

The atomic nanoscope

Andrew Steane

An ideal probe should be as small as possible so it doesn't interfere with the observation. When measuring the distribution of a light field, it seems that a single atom is up to the job.

The quest for the small has led to much ingenuity in fabricating tiny devices, and each step from micrometre to 100-nanometre to smaller scales is celebrated. One goal of such work is to reach the scale of the atom — the most sharply pointed needle one can readily conceive would have at its tip a narrow pyramid finishing with a single atom. But a sharp needle is still far from ideal as a probe: at the atomic scale it looks like a great bulky mass of material, and introduces a large disturbance into its three-dimensional environment. A radical alternative is to throw the body of the needle away altogether, and just keep the last atom. This probe would be a just a fraction of a nanometre in size in all directions — if only we could make use of it.

Guthöhrlein and co-workers[1] from the Max Planck Institute in Garching, Germany, have just taken such a step, by controlling and using a single atom to probe the structure of a standing wave of light. On page 49 of this issue they reveal the most precise measurement yet of the three-dimensional structure of a light-wave field. But this is only the first indication of what can be done with this system. The ability to control simultaneously both atomic and optical aspects of the system opens up a range of possibilities.

The Garching experiment combines the techniques of ion trapping and laser fluorescence, together with a high-quality optical cavity. The authors used a set of electrodes with oscillating voltages (known as a radio-frequency trap) to confine a single atom of calcium that has a single positive charge. They then surrounded the trap with a pair of highly reflective concave mirrors to form an optical cavity — that is, a structure inside which light will reflect to and fro forever (except for small losses), just as sound does inside the body of a reverberating musical instrument such as a violin. In this situation the light forms a standing wave between the mirrors, so there is a series of regions of brightness and darkness, separated from each other by a quarter of a wavelength (Fig. 1). Because the wavelength in these experiments was 397 nm (this is just visible to the human eye as violet light), the light field inside the cavity goes from dark to bright to dark again every 198 nm.

The aim of the experiment was to measure this structure, and also the structure in the light field perpendicular to the standing wave, which consists of the Hermite–Gauss functions known to students of optics and quantum mechanics (see Fig. 2 on page 49). To do this, several features of ion-trap experiments come to the fore. First, ion traps are tight traps: even though the electrode structure providing the trapping is on the order of 1 mm in size, the ion is confined tightly enough to restrict its movements to a region a few tens of nanometres across. This is like confining a charged coin in a region the size of a wine glass by using charged metal plates situated a mile away.

Second, to achieve this sort of confinement the ion also needs to be cold, because otherwise its natural thermal vibrations would make it explore a larger region inside

The Structure of the Potassium Channel: Molecular Basis of K + Conduction and Selectivity

Declan A. Doyle, *et al.*

Science **280**, 69 (1998);
DOI: 10.1126/science.280.5360.69

Science (print ISSN 0036-8075; online ISSN 1095-9203) is published weekly, except the last week in December, by the American Association for the Advancement of Science, 1200 New York Avenue NW, Washington, DC 20005.

The Structure of the Potassium Channel: Molecular Basis of K^+ Conduction and Selectivity

Declan A. Doyle, João Morais Cabral, Richard A. Pfuetzner, Anling Kuo, Jacqueline M. Gulbis, Steven L. Cohen, Brian T. Chait, Roderick MacKinnon*

The potassium channel from *Streptomyces lividans* is an integral membrane protein with sequence similarity to all known K^+ channels, particularly in the pore region. X-ray analysis with data to 3.2 angstroms reveals that four identical subunits create an inverted teepee, or cone, cradling the selectivity filter of the pore in its outer end. The narrow selectivity filter is only 12 angstroms long, whereas the remainder of the pore is wider and lined with hydrophobic amino acids. A large water-filled cavity and helix dipoles are positioned so as to overcome electrostatic destabilization of an ion in the pore at the center of the bilayer. Main chain carbonyl oxygen atoms from the K^+ channel signature sequence line the selectivity filter, which is held open by structural constraints to coordinate K^+ ions but not smaller Na^+ ions. The selectivity filter contains two K^+ ions about 7.5 angstroms apart. This configuration promotes ion conduction by exploiting electrostatic repulsive forces to overcome attractive forces between K^+ ions and the selectivity filter. The architecture of the pore establishes the physical principles underlying selective K^+ conduction.

Potassium ions diffuse rapidly across cell membranes through proteins called K^+ channels. This movement underlies many fundamental biological processes, including electrical signaling in the nervous system. Potassium channels use diverse mechanisms of gating (the processes by which the pore opens and closes), but they all exhibit very similar ion permeability characteristics (*1*). All K^+ channels show a selectivity sequence of $K^+ \approx Rb^+ > Cs^+$, whereas permeability for the smallest alkali metal ions Na^+ and Li^+ is immeasurably low. Potassium is at least 10,000 times more permeant than Na^+, a feature that is essential to the function of K^+ channels. Potassium channels also share a constellation of permeability characteristics that is indicative of a multi-ion conduction mechanism: The flux of ions in one direction shows high-order coupling to flux in the opposite direction, and ionic mixtures result in anomalous conduction behavior (*2*). Because of these properties, K^+ channels are classified as "long pore channels," invoking the notion that multiple ions queue inside a long, narrow pore in single file. In addition, the pores of all K^+ channels can be blocked by tetraethylammonium (TEA) ions (*3*).

Molecular cloning and mutagenesis experiments have reinforced the conclusion that all K^+ channels have essentially the same pore constitution. Without exception, all contain a critical amino acid sequence, the K^+ channel signature sequence. Mutation of these amino acids disrupts the channel's ability to discriminate between K^+ and Na^+ ions (*4*).

Two aspects of ion conduction by K^+ channels have tantalized biophysicists for the past quarter century. First, what is the chemical basis of the impressive fidelity with which the channel distinguishes between K^+ and Na^+ ions, which are featureless spheres of Pauling radius 1.33 Å and 0.95 Å, respectively? Second, how can K^+ channels be so highly selective and at the same time, apparently paradoxically, exhibit a throughput rate approaching the diffusion limit? The 10^4 margin by which K^+ is selected over Na^+ implies strong energetic interactions between K^+ ions and the pore. And yet strong energetic interactions seem incongruent with throughput rates up to 10^8 ions per second. How can these two essential features of the K^+ channel pore be reconciled?

D. A. Doyle, R. A. Pfuetzner, A. Kuo, and R. MacKinnon are in the Laboratory of Molecular Neurobiology and Biophysics and the Howard Hughes Medical Institute, Rockefeller University, 1230 York Avenue, New York, NY 10021, USA. J. M. Cabral and J. M. Gulbis are in the Laboratory of Molecular Neurobiology and Biophysics, Rockefeller University, 1230 York Avenue, New York, NY 10021, USA. S. L. Cohen and B. T. Chait are in the Laboratory of Mass Spectrometry and Gaseous Ion Chemistry, Rockefeller University, 1230 York Avenue, New York, NY 10021, USA.

*To whom correspondence should be addressed. E-mail: mackinn@rockvax.rockefeller.edu

Potassium Channel Architecture

The amino acid sequence of the K^+ channel from *Streptomyces lividans* (KcsA K^+ channel) (*5*) is similar to that of other K^+ channels, including vertebrate and invertebrate voltage-dependent K^+ channels, vertebrate inward rectifier and Ca^{2+}-activated K^+ channels, K^+ channels from plants and bacteria, and cyclic nucleotide-gated cation channels (Fig. 1). On the basis of hydrophobicity analysis, there are two closely related varieties of K^+ channels, those containing two membrane-spanning segments per subunit and those containing six. In all cases, the functional K^+ channel protein is a tetramer (*6*), typically of four identical subunits (*7*). Subunits of the two membrane-spanning variety appear to be shortened versions of their larger counterparts, as if they simply lack the first four membrane-spanning segments. Although the KcsA K^+ channel is a two membrane-spanning K^+ channel, its amino acid sequence is actually closer to those of eukaryotic six membrane-spanning K^+ channels. In particular, its sequence in the pore region, located between the membrane-spanning stretches and containing the K^+ channel signature sequence, is nearly identical to that found in the *Drosophila* (*Shaker*) and vertebrate voltage-gated K^+ channels (Fig. 1). In an accompanying paper, through a study of the KcsA K^+ channel interaction with eukaryotic K^+ channel toxins, we confirm that the KcsA pore structure is indeed very similar to that of eukaryotic K^+ channels and that its structure is maintained when it is removed from the membrane with detergent (*8*).

We have determined the KcsA K^+ channel structure from residue position 23 to 119 by x-ray crystallography (Table 1). The cytoplasmic carboxyl terminus (residues 126 to 158) was removed in the preparation and the remaining residues were disordered. The KcsA K^+ channel crystals are radiation-sensitive and the diffraction pattern is anisotropic, with reflections observed along the best and worst directions at 2.5 Å and 3.5 Å Bragg spacings, respectively. By data selection, anisotropy correction, introduction of heavy atom sites by site-directed mutagenesis, averaging, and solvent flattening, an interpretable electron density map was calculated (Fig. 2, A through C). This map was without main chain breaks and showed strong side chain density (Fig. 2C). The model was refined with data to 3.2 Å (the data set was 93 % complete to 3.2 Å with 67% completeness between 3.3 Å and 3.2 Å), maintaining highly restrained stereochemistry and keeping tight noncrystallographic symmetry restraints. The refinement procedure was

monitored by minimizing the value *R*-free (29.0%) and its separation from *R*-crystallographic (28.0%). The presence of four molecules (subunits) in the asymmetric unit of the crystal provides a very significant enhancement of the accuracy of the crystallographic analysis; first, by enabling averaging of the electron density over four crystallographically independent regions of the multiple isomorphous replacement (MIR) map, and second, by providing a powerful set of constraints on the atomic model during refinement (*9*).

The K^+ channel is a tetramer with fourfold symmetry about a central pore (Fig. 3, A and B). Like several other membrane proteins, it has two layers of aromatic amino acids positioned to extend into the lipid bilayer, presumably near the membrane-water interfaces (Fig. 3C) (*10*). Each subunit has two transmembrane α-helices connected by the roughly 30 amino acid pore region, which consists of the turret, pore helix, and selectivity filter (Fig. 3, A and B). A subunit is inserted into the tetramer such that one transmembrane helix (inner helix) faces the central pore while the other (outer helix) faces the lipid membrane. The inner helices are tilted with respect to the membrane normal by about 25° and are slightly kinked, so that the subunits open like the petals of a flower facing the outside of the cell. The open petals house the structure formed by the pore region near the extracellular surface of the membrane. This region contains the K^+ channel signature sequence, which forms the selectivity filter (*4*). The essential features of subunit packing can be appreciated by viewing the relation between the four inner helices and the four pore helices (Fig. 3D). The four inner helices pack against each other as a bundle near the intracellular aspect of the membrane, giving the appearance of an inverted teepee. The pore helices are slotted in between the poles of the teepee and are directed, with an amino-to-carboxyl sense, toward a point near the center of the channel (Fig. 3, A, B, and D). This pore helix arrangement provides many of the intersubunit contacts that hold the tetramer together and, as discussed below, is also critical in the operation of the ion conduction pore.

Sequence conservation among K^+ channels (including ones with two and six membrane-spanning segments), as well as cyclic nucleotide-gated cation channels, is strongest for the amino acids corresponding to the pore region and the inner helix. Even Na^+ and Ca^{2+} channels show distant relatedness over these segments. The teepee architecture of the K^+ channel pore likely will be a general feature of all of these cation channels, with four inner helices arranged like the poles of a teepee, four pore helices, and a selectivity filter—tuned to select the appropriate cation—located close to the extracellular surface.

This structure of the KcsA K^+ channel is in excellent agreement with results from functional and mutagenesis studies on *Shaker* and other eukaryotic K^+ channels (Fig. 4). The pore-region of K^+ channels was first defined with pore-blocking scorpion toxins (*11*). These inhibitors interact with amino acids (Fig. 4, white) comprising the broad extracellular-facing entryway to the pore (*12*). The impermeant organic cation TEA blocks K^+ channels from both sides of the membrane at distinct sites (*13*). Amino acids interacting with externally and internally applied TEA are located just external to (Fig. 4, yellow) and internal to (Fig. 4, mustard) the structure formed by the signature sequence amino acids (*14, 15*). Alteration of the signature sequence amino acids (Fig. 4, red main chain atoms) disrupts K^+ selectivity (*4*). Amino acids close to the intracellular opening on the *Shaker* K^+ channel map to the inner helix on the KcsA K^+ channel (*16*). Interestingly, exposure to the cytoplasm of the region above the inner helix bundle (Fig. 4, pink side chains) requires an open voltage-dependent gate, whereas the region at or below the bundle (Fig. 4, green side chains) is exposed whether or not the gate was open. The correlation between the transition zone for gate-dependent exposure to the cytoplasm in the *Shaker* K^+ channel and the inner helix bundle in this structure has implications for mechanisms of gating in K^+ channels.

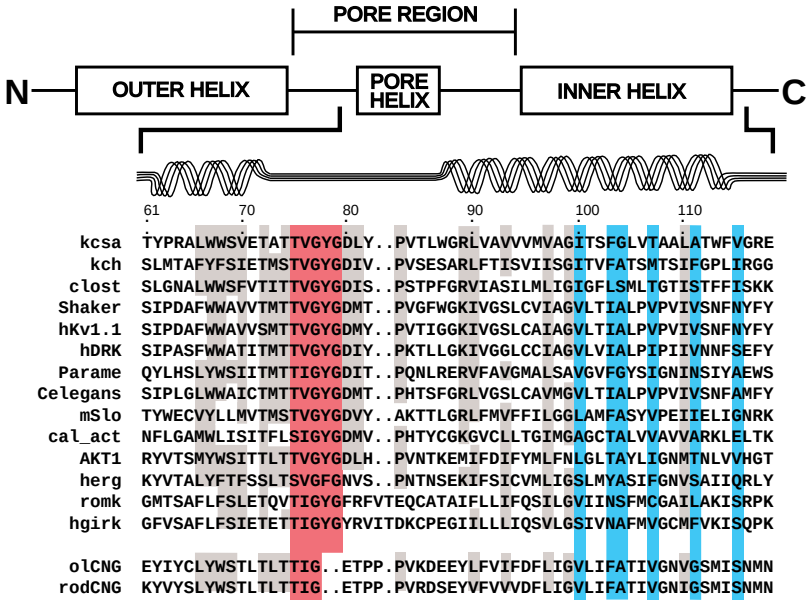

Fig. 1. Sequence alignment of selected K^+ channels and cyclic nucleotide-gated channels. The numbering and secondary structural elements for the *Streptomyces lividans* K^+ channel (KcsA) is given above the sequences. Selectivity filter, red; lining of the cavity and inner pore, blue; residues in which the nature of the side chain is preserved (>50% similarity), grey. The sequences are: KcsA, *Streptomyces lividans*, accession number (acc) PIR S60172; kch, *Escherichia coli*, acc GenBank U24203; clost, *Clostridium acetobutylicum* (Genome Therapeutics Corp.); Shaker, *Drosophila melanogaster*, acc PIR S00479; hKv1.1, *Homo sapiens*, acc Swissprot Q09470; hDRK, *H. sapiens*, acc PIR S31761; Parame, *Paramecium tetraaurelia*, acc GenBank U19908; Celegans, *Caenorhabditis elegans*, acc GenBank AF005246; mSlo, *Mus musculus*, acc PIR A48206; cal_act, *H. sapiens*, acc GenBank AF031815; AKT1, *Arabidopsis thaliana*, acc PIR S62694; herg, *H. sapiens*, acc PIR I38465; romk, *Rattus norvegicus*, acc Swissprot P35560; hgirk, *H. sapiens*, acc GenBank S78684; olCNG, *H. sapiens*, acc Swissprot Q16280; rodCNG, *H. sapiens*, acc PIR A42161. The last two sequences, separate from the rest, are from cyclic nucleotide–gated channels, which are not K^+ selective.

General Properties of the Ion Conduction Pore

As might have been anticipated for a cation channel, both the intracellular and extracellular entryways are negatively charged by acidic amino acids (Fig. 5A, red), an effect that would raise the local concentration of cations while lowering the concentration of anions. The overall length of the pore is 45 Å, and its diameter varies along its distance (Fig. 5B). From inside the cell (bottom) the pore begins as a tunnel 18 Å in length (the internal pore) and then opens into a wide cavity (~10 Å across) near the middle of the membrane. A K^+ ion could move throughout the internal pore and cavity and still remain mostly hydrated. In contrast, the selectivity filter separating the cavity

from the extracellular solution is so narrow that a K^+ ion would have to shed its hydrating waters to enter. The chemical composition of the wall lining the internal pore and cavity is predominantly hydrophobic (Fig. 5A, yellow). The selectivity filter, on the other hand, is lined exclusively by polar main chain atoms belonging to the signature sequence amino acids. The distinct mechanisms operating in the cavity and internal pore versus the selectivity filter will be discussed below, but first we introduce the determination of K^+ ion positions in the pore.

Potassium channels exclude the smaller alkali metal cations Li^+ (radius 0.60 Å) and Na^+ (0.95 Å) but allow permeation of the larger members of the series Rb^+ (1.48 Å) and Cs^+ (1.69 Å). In fact, Rb^+ is nearly a perfect K^+ (1.33 Å) analog because its size and permeability characteristics are very similar to those of K^+. Because they are more electron dense than K^+, Rb^+ and Cs^+ allow visualization of the locations of permeant ions in the pore. By difference electron density maps calculated with data from crystals transferred into Rb^+-containing (Fig. 6a) or Cs^+-containing (Fig. 6b) solutions, multiple ions are well defined in the pore. The selectivity filter contains two ions (inner and outer ions) located at opposite ends, about 7.5 Å apart (center to center). In the Rb^+ difference map, there actually are two partially separated peaks at the inner aspect of the selectivity filter. These peaks are too close to each other (2.6 Å) to represent two simultaneously occupied ion binding sites. We suspect that they represent a single ion (on average) in rapid equilibrium between adjacent sites. The single inner ion peak in the Cs^+ difference map undoubtedly reflects the lower resolution at which the map was calculated (to 5 Å for Cs^+ versus 4.0 Å for Rb^+), because the Rb^+ difference map, when calculated at the same lower resolution, also shows only a single peak at the Cs^+ position. The Rb^+ positions correspond to strong peaks (pre-

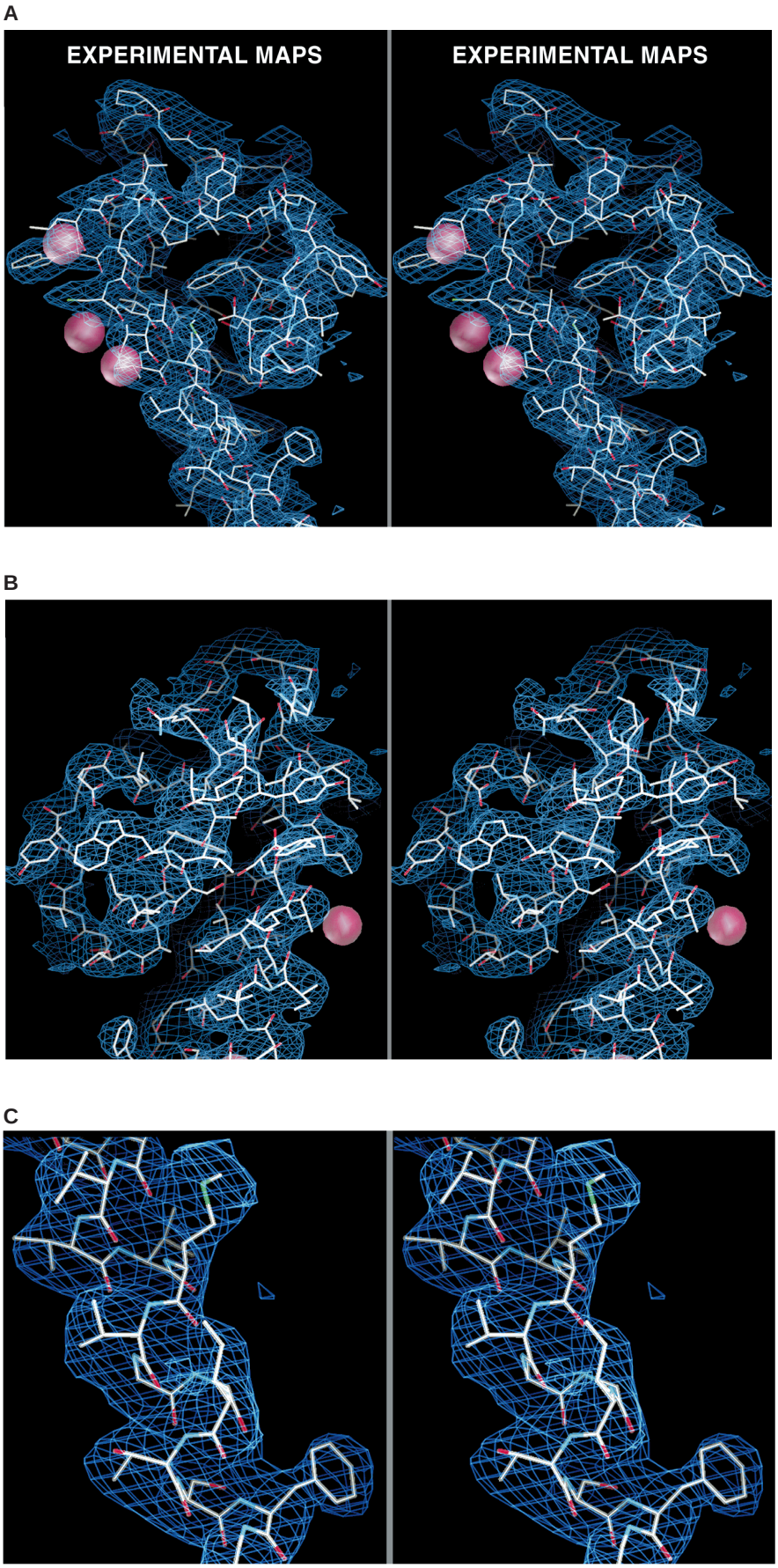

Fig. 2. Experimental electron density map. Stereoviews of the experimental electron-density map contoured at 1 σ covering nearly an entire subunit (removed from the tetramer) of the final model. The map was calculated at 3.2 Å resolution with the following Fourier coefficients: native-sharpened amplitudes and MIR solvent flattened averaged phases. (**A**) Foreground: map showing inner helix, loop structures and selectivity filter; background: the pore helix and outer helix. CPK spheres show positions of mercury atoms used as residue markers (from the top, marked residues are Leu^{86}, Leu^{90} and Val^{93}). (**B**) Alternative view. Foreground: pore helix and part of outer helix; background: selectivity filter and turret. CPK sphere marks position of Ala^{42}. (**C**) Close up view of electron density.

sumably, K^+ ions) in a high contour native electron density map (not shown). Thus, the selectivity filter contains two K^+ ions. A third weaker peak is located below the selectivity filter at the center of the large cavity in the Rb^+ difference map (Fig. 6a, cavity ion) and in the Cs^+ difference map at a lower contour (not shown). Electron density at the cavity center is prominent in MIR maps, even prior to averaging (Fig. 6c, lower diffuse peak). The difference electron density maps show this to be related to the presence of one or more poorly localized cations situated at least 4 Å away from the closest protein groups.

The Cavity and Internal Pore

Why is there a 10 Å diameter cavity in the center of the channel with an ion in it (Fig. 5B and Fig. 6)? Electrostatic calculations show that when an ion is moved along a narrow pore through a membrane, it must cross an energy barrier that is maximum at the membrane center (*17*). The electrostatic field emanating from a cation polarizes its environment, bringing the negative ends of dipoles closer to it and thereby stabilizing it. At the bilayer center, the polarizability of the surround-

Table 1. Summary of data collection and refinement statistics. Crystals (space group C2: a = 128.8 Å, b = 68.9 Å, c = 112.0 Å, β = 124.6°) were flash-frozen by being transferred directly from the crystal mother liquor to a stream of boiled-off nitrogen (*24*). Because crystals of the mutant L90C diffracted significantly better than wild-type protein crystals, the former were used for native data collection. Data were collected from multiple crystals, and six sets were selected and merged to form the native data set used for structure determination. Mercury derivatives were obtained by direct addition of methyl mercury to the crystallization solution of cysteine mutant crystals. MALDI-TOF mass spectrometry confirmed 60 to 90% derivatization of crystals prior to data collection. All data were collected at Cornell High Energy Synchrotron Source (CHESS), station A1, with the Princeton 2K CCD (*25*). Data were processed with DENZO and SCALEPACK (*26*) and the CCP4 package (*27*). Heavy atom positions were determined with SHELX-97 (*28*) and cross-difference Fourier analysis. These positions confirmed the fourfold noncrystallographic symmetry observed in the self-rotation Patterson function and allowed the determination of initial orientation matrices. An initial model (90% complete) was built into a solvent flattened (64% solvent content), fourfold averaged electron density map with the program O (*29*). The tracing of the model was facilitated by the use of the mercury atom positions as residue markers. L86C was used solely for this purpose. After torsional refinement (with strict fourfold noncrystallographic symmetry constraints) with X-PLOR 3.851 (*30*), this model was used in the anisotropic scaling [sharpening (*31*)] of the native data with X-PLOR. The structure factor sigma values were also rescaled appropriately, and the corrected data were used for all subsequent procedures. Fourfold averaging, solvent flattening, and phase extension were applied in DM (*32*), resulting in a marked improvement of the electron density that allowed correction of the model and the building of additional residues. Refinement consisted of rounds of positional (in the initial stages phase information was also included as a restraint) and grouped B-factor refinement in X-PLOR. Fourfold noncrystallographic symmetry was highly restrained with the force constant for positional restraints set as 1000 kcal/mol/Å^2. The diffuse ion cloud described in the text was initially modeled as one or more K^+ ions and several water molecules; however, the results were unsatisfactory. Therefore, this and other strong unmodelled density present in solvent-flattened maps (no averaging included) was Fourier back-transformed, scaled, and included in the refinement procedure as partial structure factors. The final model includes amino acids 23 to 119 of each chain. The following residues were truncated: Arg^{27} to Cβ, Ile^{60} to Cγ, Arg^{64} to Cβ, Glu^{71} to Cβ, and Arg^{117} to Nε. The stereochemistry is strongly restrained, with no outliers on the Ramachandran plot. The high B-factor values reflect the intensity decay of the data beyond 4 Å.

Data collection and phasing

Data set	Resolution (Å)	Redundancy	Completeness overall/outer (%)	R_{merge}*	Phasing power†	R-Cullis‡
L90C-a	15.0–3.7	3.5	91.3/93.3	0.071	1.61	0.70
L90C-b	15.0–3.7	7.0	91.5/94.1	0.083	1.87	0.50
V93C	15.0–3.7	4.1	98.3/99.1	0.075	1.35	0.63
A32C	15.0–4.0	2.3	84.1/83.8	0.076	1.45	0.66
A29C	15.0–5.0	2.7	73.9/74.0	0.063	1.03	0.85
A42C	15.0–6.5	2.0	90.7/90.3	0.057	0.97	0.81
L86C	30.0–6.0	2.3	58.7/58.9	0.057	—	—
					$I/\sigma I$	% of measured data with $I/\sigma I > 2$
Native	30.0–3.2	6.1	93.3%	0.086	15.8	75
Outer Shell	3.3–3.2	2.3	66.6%	0.286	3.9	50

Anisotropic correction

	Average F.O.M‖ (30.0–3.2 Å)	Average F.O.M‖ (3.4–3.2 Å)
Before sharpening¶	0.76	0.55
After sharpening¶	0.83	0.64

Refinement		*Root-mean-square deviation of*	
Resolution:	10.0–3.2 Å	Bond angles:	1.096°
R-cryst.§:	28.0%	Bond lengths:	0.005 Å
R-free§:	29.0%	Ncs related atoms:	0.006 Å
No. of reflections with $\|F\|/\sigma\|F\| > 2$:	12054	B-factor for ncs related atoms:	10 Å^2
No. of protein atoms:	710 per subunit	B-factor for non-bonded atoms:	36 Å^2
No. of ligand atoms:	1 water, 3 K^+ ions		
Mean B-factor for main-chain atoms:	90 Å^2		
Mean B-factor for side-chain atoms:	110 Å^2		

*$R_{merge} = \Sigma\Sigma|I-Ij|/\Sigma I$. †Phasing power = $\langle|F_h|\rangle/\langle E\rangle$. ‡$R$-Cullis = $\Sigma\|F_{ph} \pm F_p| - |F_{hc}\|/\Sigma|F_{ph} \pm F_p|$, only for centric data. §R-cryst. = $\Sigma|F_p - F_{p(calc)}|/\Sigma|F_p|$, R-free the same as R-cryst, but calculated on 10% of data selected in thin resolution shells and excluded from refinement. ‖Figure of merit. ¶In both cases, fourfold averaging and solvent flattening were applied; Ij is the observed intensity, I is the average intensity, F_h is the root-mean-square heavy-atom structure factor, E is the lack of closure error, F_{ph} is the structure factor for the derivative, F_p is the structure factor for the native, F_{hc} is the calculated structure factor for the heavy atom, and $F_{p(calc)}$ is the calculated native structure factor.

ing medium is minimal and therefore the energy of the cation is highest. Thus, simple electrostatic considerations allow us to understand the functional significance of the cavity and its strategic location. The cavity overcomes the electrostatic destabilization resulting from the low dielectric bilayer by simply surrounding an ion with polarizable water. A second feature of the K^+ channel structure also stabilizes a cation at the bilayer center. The four pore helices point directly at the center of the cavity (Fig. 3, A, B, and D). The amino to carboxyl orientation of these helices will impose a negative electrostatic (cation attractive) potential via the helix dipole effect (*18*). The ends of the helices are rather far (~8 Å) from the cavity center, but all four contribute to the effect. Therefore, two properties of the structure, the aqueous cavity and the oriented helices, help to solve a fundamental physical problem in biology—how to lower the electrostatic barrier facing a cation crossing a lipid bilayer. Thus, the diffuse electron density in the cavity center (Fig. 6C) likely reflects a hydrated cation cloud rather than an ion binding site (Fig. 7).

Alternatively, the channel could have overcome the destabilizing electrostatic effects of the bilayer center by lining the entire pore with a polarizable surface, putting ion binding sites along its entire length. But the structure shows that, with the exception of the selectivity filter, the pore lining is mainly hydrophobic, a general property of K^+ channels (Fig. 1). This conclusion was anticipated by the landmark experiments of Armstrong, which showed that hydrophobic cations bind in

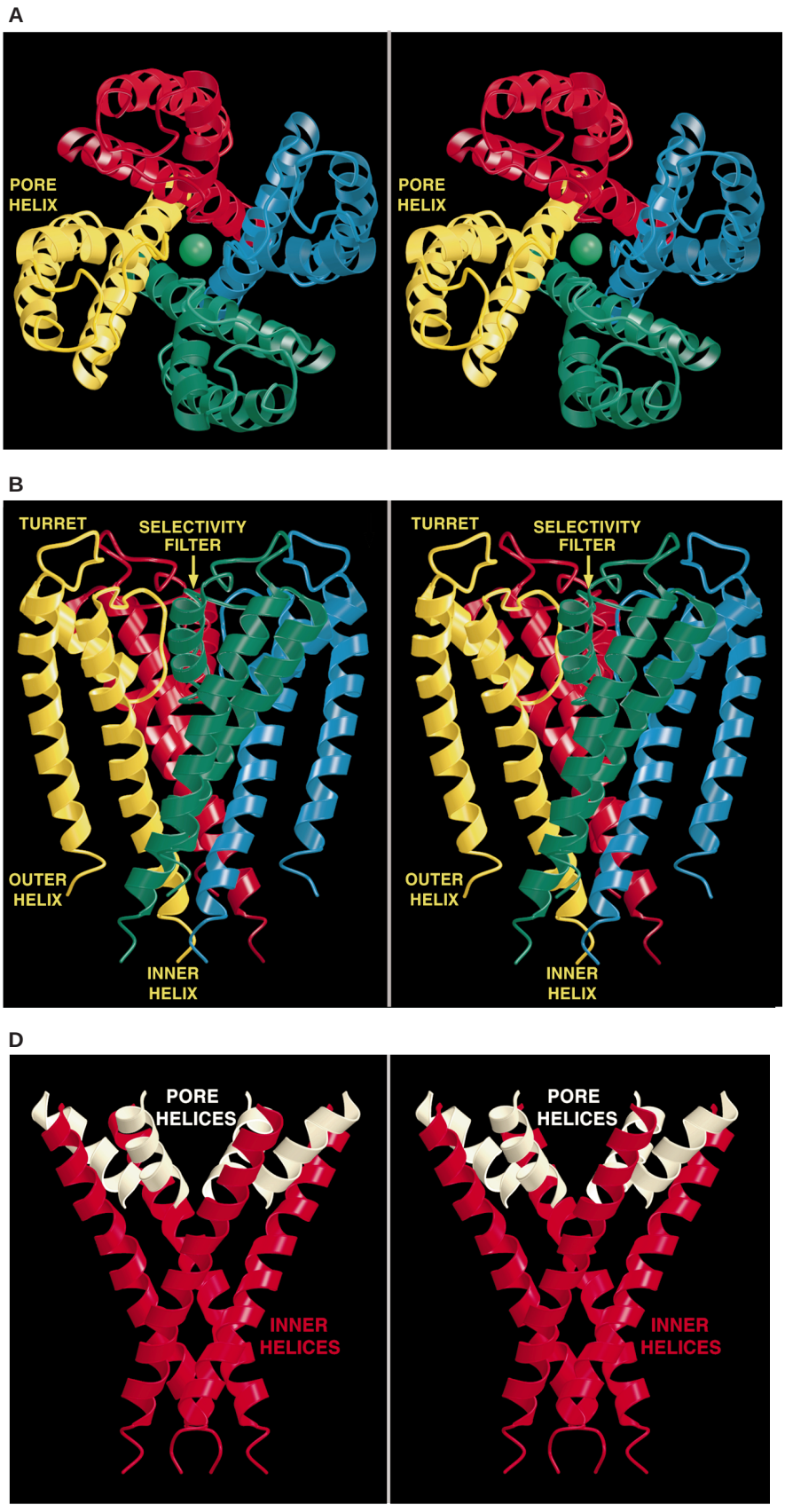

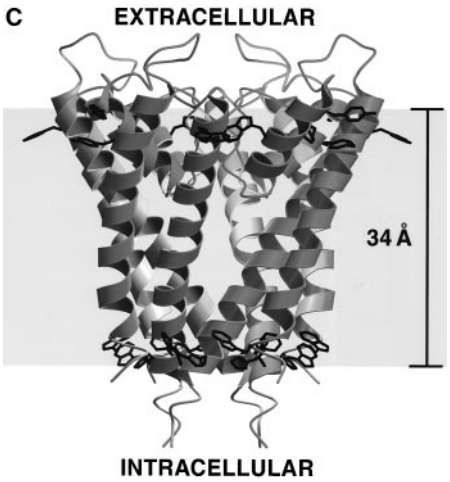

Fig. 3. Views of the tetramer. (**A**) Stereoview of a ribbon representation illustrating the three-dimensional fold of the KcsA tetramer viewed from the extracellular side. The four subunits are distinguished by color. (**B**) Stereoview from another perspective, perpendicular to that in (A). (**C**) Ribbon representation of the tetramer as an integral-membrane protein. Aromatic amino acids on the membrane-facing surface are displayed in black. (**D**) Inverted teepee architecture of the tetramer. These diagrams were prepared with MOLSCRIPT and RASTER-3D (*33*).

the pore of K^+ channels (*3*). What is the significance of the hydrophobic lining? We suggest that it would be counterproductive to achieving a high throughput of K^+ ions were the lining of the channel to interact strongly with ions outside of the selectivity filter. The hydrophobic lining presents a relatively inert surface to a diffusing ion over most of the length of the pore.

In summary, the inner pore and cavity lower electrostatic barriers without creating deep energy wells. The structural and chemical design of this part of the pore ensure a low resistance pathway from the cytoplasm to the selectivity filter, facilitating a high throughput. Functional experiments on K^+ channels support this conclusion. When TEA from the cytoplasm migrates to its binding site at the top of the cavity [>50% of the physical distance across the membrane (Figs. 4 and 5)], it traverses only about 20% of the transmembrane voltage difference (*15*). Thus, 80% of the transmembrane voltage is imposed across the relatively short selectivity filter. The rate limiting steps for a K^+ ion traversing the channel are thereby limited to this short distance. In effect, the K^+ channel has thinned the relevant transmembrane diffusion distance to a mere 12 Å.

The Selectivity Filter

The atomic model for the K^+ channel selectivity filter was based on the experimental electron density map, which showed a continuous ridge of electron density attributable to the main chain, as well as strong Val and Tyr side chain density directed away from the pore (Fig. 8A). We also used K^+ ion positions defined by difference Fourier analysis (Figs. 6 and 8A, yellow density) and our knowledge of alkali metal cation coordination in small molecules. The side chain locations preclude their direct participation in ion coordination, leaving this function to the

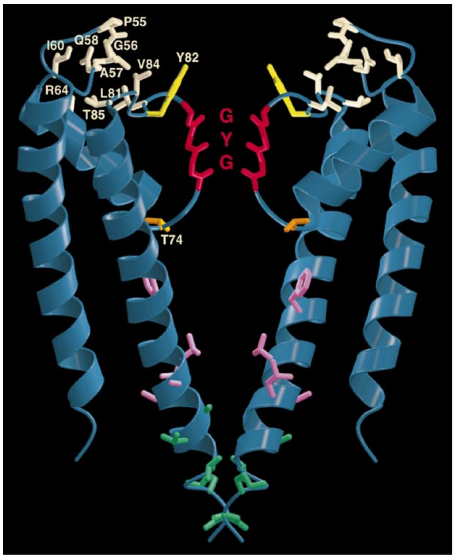

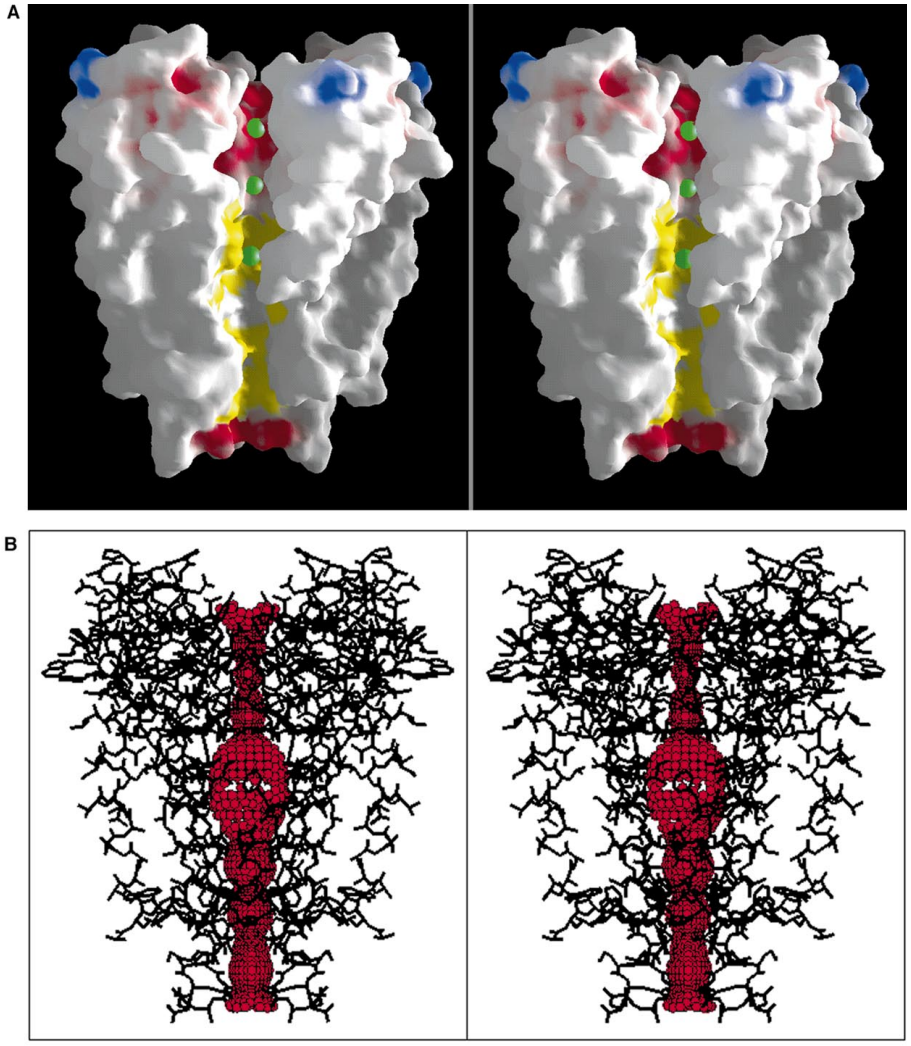

Fig. 4 (**above**)**.** Mutagenesis studies on *Shaker*: Mapping onto the KcsA structure. Mutations in the voltage-gated *Shaker* K^+ channel that affect function are mapped to the equivalent positions in KcsA based on the sequence alignment. Two subunits of KcsA are shown. Mutation of any of the white side chains significantly alters the affinity of agitoxin2 or charybdotoxin for the *Shaker* K^+ channel (*12*). Changing the yellow side chain affects both agitoxin2 and TEA binding from the extracellular solution (*14*). This residue is the external TEA site. The mustard-colored side chain at the base of the selectivity filter affects TEA binding from the intracellular solution [the internal TEA site (*15*)]. The side chains colored green, when mutated to cysteine, are modified by cysteine-reactive agents whether or not the channel gate is open, whereas those colored pink react only when the channel is open (*16*). Finally, the residues colored red (GYG, main chain only) are absolutely required for K^+ selectivity (*4*). This figure was prepared with MOLSCRIPT and RASTER-3D. **Fig. 5** (**right**)**.** Molecular surface of KcsA and contour of the pore. (**A**) A cutaway stereoview displaying the solvent-accessible surface of the K^+ channel colored according to physical properties. Electrostatic potential was calculated with the program GRASP, assuming an ionic strength equivalent to 150 mM KCl and dielectric constants of 2 and 80 for protein and solvent, respectively. Side chains of Lys, Arg, Glu, and Asp residues were assigned single positive or negative charges as appropriate, and the surface coloration varies smoothly from blue in areas of high positive charge through white to red in negatively charged regions. The yellow areas of the surface are colored according to carbon atoms of the hydrophobic (or partly so) side chains of several semi-conserved residues in the inner vestibule (Thr^{75}, Ile^{100}, Phe^{103}, Thr^{107}, Ala^{108}, Ala^{111}, Val^{115}). The green CPK spheres represent K^+ ion positions in the conduction pathway. (**B**) Stereoview of the entire internal pore. Within a stick model of the channel structure is a three-dimensional representation of the minimum radial distance from the center of the channel pore to the nearest van der Waals protein contact. The display was created with the program HOLE (*34*).

main chain atoms. The precise orientation of individual carbonyl oxygens cannot be discerned at the resolution of this x-ray analysis, but we propose that they are directed inward to account for K^+ ion coordination (Fig. 8B). A single water molecule (the only one modeled in the structure) located between the two K^+ ions in the selectivity filter was justified by the presence of a strong electron density peak in the experimental map, which was never associated with an ion peak in the difference Fourier maps (*19*).

The structure of the selectivity filter exhibits two essential features. First, the main chain atoms create a stack of sequential oxygen rings and thus afford numerous closely spaced sites of suitable dimensions for coordinating a dehydrated K^+ ion. The K^+ ion thus has only a very small distance to diffuse from one site to the next within the selectivity filter. The second important structural feature of the selectivity filter is the protein packing around it. The Val and Tyr side chains from the V-G-Y-G sequence point away from the pore and make specific interactions with amino acids from the tilted pore helix. Together with the pore helix Trp residues, the four Tyr side chains form a massive sheet of aromatic amino acids, twelve in total, that is positioned like a cuff around the selectivity filter (Fig. 8C). The hydrogen bonding, for example between the Tyr hydroxyls and Trp nitrogens, and the extensive van der Waals contacts within the sheet, offer the immediate impression that this structure behaves like a layer of springs stretched radially outward to hold the pore open at its proper diameter.

How does the K^+ channel structure account for its prodigious ion selective properties? When an ion enters the selectivity filter, it evidently dehydrates (nearly completely). To compensate for the energetic cost of dehydration, the carbonyl oxygen atoms must take the place of the water oxygen atoms, come in very close contact with the ion, and act like surrogate water (*20, 21*). The structure reveals that the selectivity filter is held open as if to prevent it from accommodating a Na^+ ion with its smaller radius. We propose that a K^+ ion fits in the filter precisely so that the energetic costs and gains are well balanced. The structure of the selectivity filter with its molecular springs holding it open prevents the carbonyl oxygen atoms from approaching close enough to compensate for the cost of dehydration of a Na^+ ion.

In about 150 mM K^+, the selectivity filter contains two K^+ ions (Figs. 6 and 8). The ions are located at opposite ends of the selectivity filter, separated by about 7.5 Å, roughly the average distance between K^+ ions in a 4 M KCl solution, and in the selectivity filter there are no intervening Cl^- anions to balance the charge. We therefore conclude that the selectivity filter attracts and concentrates K^+ ions. But how does such a selectivity filter ever conduct ions? The structure implies that a single K^+ ion would be held very tightly, but that the presence of two K^+ ions results in mutual repulsion, hence their locations near opposite ends of the selectivity filter. Thus, when a second ion enters, the attractive force between a K^+ ion and the selectivity filter becomes perfectly balanced by the repulsive force between ions, and this is what allows conduction to occur. This picture accounts for both a strong interaction between K^+ ions and the selectivity filter and a high throughput mediated by electrostatic repulsion. On the basis of functional measurements, the same concept of destabilization by multiple ion occupancy has been proposed for Ca^{2+} channels (*22*) and for K^+ channels (*23*) and may be a general property of all selective ion channels.

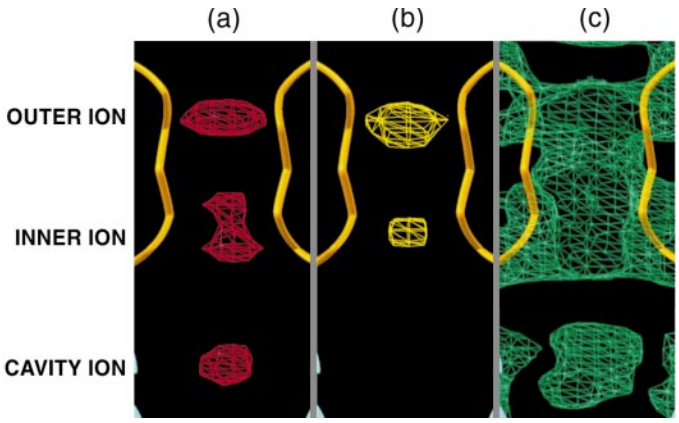

Fig. 6. Identification of permeant ion positions in the pore. (**a**) A Rb^+ difference Fourier map calculated to 4.0 Å and contoured at 6 σ identifies two strong peaks corresponding to ions in the selectivity filter (inner and outer ions) and a weaker peak corresponding to ions in the cavity (cavity ion). The inner ion density has two closely spaced peaks. (**b**) A Cs^+ difference Fourier map calculated to 5.0 Å and contoured at 6 σ shows the inner and outer ion peaks in the selectivity filter. Both difference Fourier maps were calculated with Fourier coefficients: F(soak) – F(native-unsharpened) and MIR phases. (**c**) Electron density map contoured at 1 σ showing diffuse density at the cavity ion position. This map was calculated with the following Fourier coefficients: unsharpened native amplitudes and MIR solvent-flattened phases (no averaging information was included).

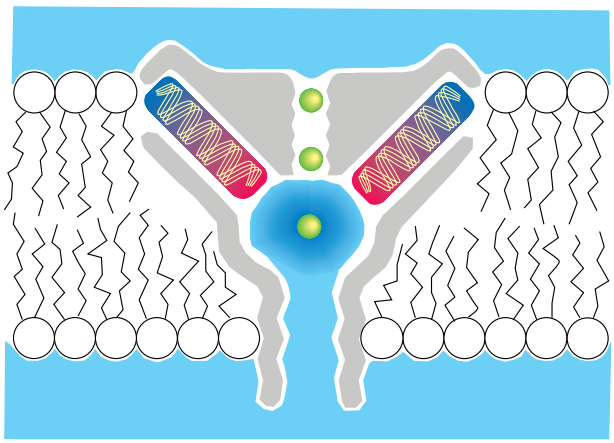

Fig. 7. Two mechanisms by which the K^+ channel stabilizes a cation in the middle of the membrane. First, a large aqueous cavity stabilizes an ion (green) in the otherwise hydrophobic membrane interior. Second, oriented helices point their partial negative charge (carboxyl end, red) towards the cavity where a cation is located.

Summary

We propose that the following principles underlie the structure and operation of K^+ channels. (i) The pore is constructed of an inverted teepee, with the selectivity filter held at its wide end. This architecture also describes the pore of cyclic nucleotide–gated channels and probably Na^+ and Ca^{2+} channels as well. (ii) The narrow selectivity filter is only 12 Å long, whereas the remainder of the pore is wider and has a relatively inert hydrophobic lining. These structural and chemical properties favor a high K^+ throughput by minimizing the distance over which K^+ interacts strongly with the channel. (iii) A large water-filled cavity and helix dipoles help to overcome the high electrostatic energy barrier facing a cation in the low dielectric membrane center. (iv) The K^+ selectivity filter is lined by carbonyl oxygen atoms, which provide multiple closely spaced sites. The filter is constrained in an opti-

mal geometry so that a dehydrated K^+ ion fits with proper coordination but the Na^+ ion is too small. (v) Two K^+ ions at close proximity in the selectivity filter repel each other. The repulsion overcomes the otherwise strong interaction between ion and protein and allows rapid conduction in the setting of high selectivity.

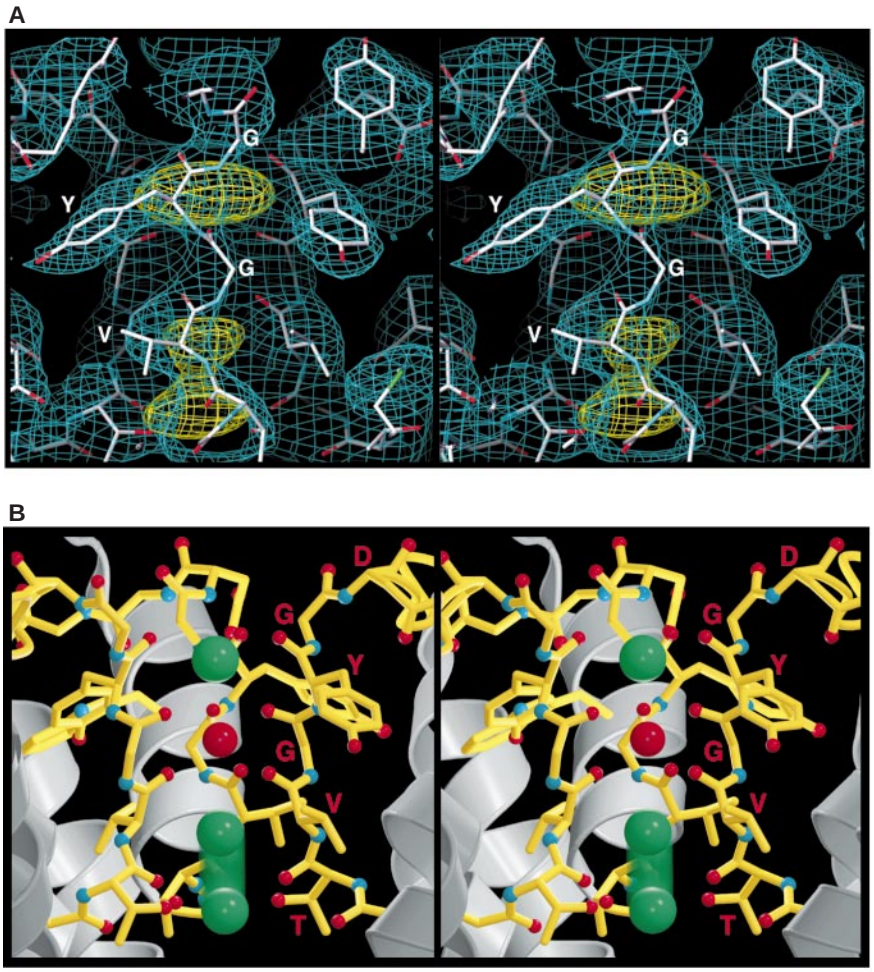

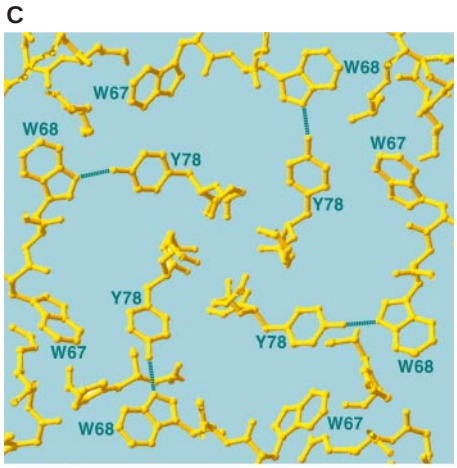

Fig. 8. Detailed views of the K^+ channel selectivity filter. (**A**) Stereoview of the experimental electron density (green) in the selectivity filter. The map was calculated with native-sharpened amplitudes and MIR-solvent-flattened-averaged phases. The selectivity filter of three subunits is shown as a stick representation with several signature sequence residues labeled. The Rb^+ difference map (yellow) is also shown. (**B**) Stereoview of the selectivity filter in a similar orientation to (A) with the chain closest to the viewer removed. The three chains represented are comprised of the signature sequence amino acids Thr, Val, Gly, Tyr, Gly running from bottom to top, as labeled in single-letter code. The Val and Tyr side chains are directed away from the ion conduction pathway, which is lined by the main chain carbonyl oxygen atoms. Two K^+ ions (green) are located at opposite ends of the selectivity filter, roughly 7.5 Å apart, with a single water molecule (red) in between. The inner ion is depicted as in rapid equilibrium between adjacent coordination sites. The filter is surrounded by inner and pore helices (white). Although not shown, the model accounts for hydrogen bonding of all amide nitrogen atoms in the selectivity filter except for that of Gly^{77}. (**C**) A section of the model perpendicular to the pore at the level of the selectivity filter and viewed from the cytoplasm. The view highlights the network of aromatic amino acids surrounding the selectivity filter. Tyrosine-78 from the selectivity filter (Y78) interacts through hydrogen bonding and van der Waals contacts with two Trp residues (W67, W68) from the pore helix.

REFERENCES AND NOTES

1. B. Hille, *Ionic Channels of Excitable Membranes* (Sinauer, Sunderland, MA, ed. 2, 1992).
2. A. L. Hodgkin and R. D. Keynes, *J. Physiol. (London)* **128**, 61 (1955); S. Hagiwara, S. Miyazaki, S. Krasne, S. Ciani, *J. Gen. Physiol.* **70**, 269 (1977); B. Hille and W. Schwartz, *ibid.* **72**, 409 (1978); J. Neyton and C. Miller, *ibid.* **92**, 549 (1988).
3. C. M. Armstrong and L. Binstock, *J. Gen. Physiol.* **48**, 859 (1965); C. M. Armstrong, *ibid.* **50**, 491 (1966); *ibid.* **54**, 553 (1969); *ibid.* **58**, 413 (1971).
4. L. Heginbotham, T. Abramson, R. MacKinnon, *Science* **258**, 1152 (1992); L. Heginbotham, Z. Lu, T. Abramson, R. MacKinnon, *J. Biophys.* **66**, 1061 (1994).
5. H. Schempf *et al.*, *EMBO J.* **14**, 5170 (1995); L. Heginbothan, E. Odessey, C. Miller, *Biochemistry* **36**, 10335 (1997); D. Marien Cortes and E. Perozo, *ibid.*, p. 10343.
6. R. MacKinnon, *Nature* **350**, 232 (1991).
7. Certain K^+ channels contain the equivalent of two subunits in a single open reading frame. These are thought to form the tetramer through the assembly of two dimer subunits [K. A. Ketchum *et al.*, *Nature* **376**, 690 (1995)].
8. R. MacKinnon *et al.*, *Science* **280**, 106 (1998).
9. G. J. Kleywegt and R. J. Read, *Structure* **5**, 1557 (1998).
10. J. Deisenhofer *et al.*, *Nature* **318**, 618 (1985); S. W. Cowan *et al.*, *ibid.* **358**, 727 (1992); A. Kreusch and G. E. Schulz, *J. Mol. Biol.* **243**, 891 (1994).
11. R. MacKinnon and C. Miller, *Science* **245**, 1382 (1989).
12. R. MacKinnon, L. Heginbotham, T. Abramson, *Neuron* **5**, 767 (1990); M. Stocker and C. Miller, *Proc. Natl. Acad. Sci. U.S.A.* **91**, 9509 (1994); S. A. N. Goldstein, D. J. Pheasant, C. Miller, *Neuron* **12**, 1377 (1994); P. Hidalgo and R. MacKinnon, *Science* **268**, 307 (1995); J. Aiyar *et al.*, *Neuron* **15**, 1169 (1995); D. Naranjo and C. Miller, *ibid.* **16**, 123 (1996); R. Ranganathan, J. H. Lewis, R. MacKinnon, *ibid.*, p. 131; A. Gross and R. MacKinnon, *ibid.*, p. 399.
13. C. M. Armstrong and B. Hille, *J. Gen. Physiol.* **59**, 388 (1972).
14. R. MacKinnon and G. Yellen, *Science* **250**, 276 (1990).
15. G. Yellen, M. E. Jurman, T. Abramson, R. MacKinnon, *ibid.* **251**, 939 (1991).
16. Y. Liu, M. Holmgren, M. E. Jurman, G. Yellen, *Neuron* **19**, 175 (1997).
17. V. A. Parsegian, *Ann. N.Y. Acad. Sci.* **264**, 161 (1975).
18. D. Sali, M. Bycroft, A R. Fersht, *Nature* **335**, 740 (1988); J. Aqvist, H. Luecke, F. A. Quiocho, A. Warshel, *Proc. Natl. Acad. Sci. U.S.A.* **88**, 2026 (1991); D. J. Lockhart and P. S. Kim, *Science* **257**, 947 (1992); *ibid.* **260**, 198 (1993).
19. The temperature factors for Val^{76} and Gly^{77} main chain atoms (but not side chain atoms) refined to higher values than for neighboring atoms. This result can be explained by the difference Fourier analysis, which shows alternative positions of the inner K^+ ion in the selectivity filter and therefore, by inference, alternative conformations of the coordinating main chain atoms, depending on the location of the K^+ ion.
20. F. Bezanilla and C. M. Armstrong, *J. Gen. Physiol.* **60**, 588 (1972).
21. B. Hille, *ibid.* **61**, 669 (1973).
22. W. Almers and E. W. McCleskey, *J. Physiol. (London)* **353**, 585 (1984); P. Hess and R. W. Tsien, *Nature* **309**, 453 (1984).
23. J. Neyton and C. Miller, *J. Gen. Physiol.* **92**, 569 (1988).
24. The KcsA gene was subcloned into pQE60 (Qiagen) vector and expressed in *E. coli* XL-1 Blue cells upon induction with 1-β-D-thiogalactopyranoside. The carboxyl-terminal histidine tagged protein was extracted by homogenization and solubilization in 40 mM decylmaltoside (Anatrace). The KcsA channel

was purified on a cobalt affinity column. Thirty-five carboxyl terminal amino acids were cleaved by chymotrypsin proteolysis. The truncated channel was purified to homogeneity by gel filtration and the detergent exchanged in a final dialysis step against 5 mM N,N-dimethyldodecylamine-N-oxide (LDAO). Crystals were grown at 20°C with the sitting drop method by mixing equal volumes of protein solution [5 to 10 mg/ml, 150 mM KCl, 50 mM tris (pH 7.5), and 2 mM dithiothreitol] with reservoir mixture [200 mM $CaCl_2$, 100 mM Hepes (pH 7.5), and 48% PEG 400]. Through the entire preparation, the channel protein was maintained in solutions containing 150 mM KCl. For definition of K^+ sites, crystals were transferred into solutions where 150 mM KCl was replaced by 150 mM RbCl or 150 mM CsCl.

25. M. W. Tate *et al.*, *J. Appl. Crystallogr.* **28**, 196 (1995); D.J. Thiel *et al.*, *Rev. Sci. Instrum.* **67**, 1 (1996).
26. Z. Otwinowski, in *Data Collection and Processing*, L. Sawyer and S. Bailey, Eds. (Science and Engineering Research Council Daresbury Laboratory, Daresbury, UK, 1993), pp. 56–62.
27. Collaborative Computational Project 4 (CCP4), *Acta Crystallogr.* **D50**, 760 (1994).
28. G. M. Sheldrick, *ibid.* **46**, 467 (1990).
29. T. A. Jones, J. Y. Zou, J. Y. Cowan, M. Kjeldgaard, *ibid.* **A47**, 110 (1991).
30. A. T. Brunger, X-PLOR (Version 3.851) Manual (The Howard Hughes Medical Institute and Department of Molecular Biophysics and Biochemistry, Yale University, New Haven, CT).
31. S. J. Gamblin, D. W. Rodgers, T. Stehle, Proceedings of the CCP4 study weekend, Daresbury Laboratory (1996), pp. 163–169.
32. K. Y. J. Zhang and P. Main, *Acta Crystallogr.* **A46**, 377.
33. P. J. Kraulis, *J. Appl. Crystallogr.* **24**, 946 (1991).
34. O. S. Smart, J. G. Neduvelil, X. Wang, B. A. Wallace, M. P. Sansom, *J. Mol. Graphics* **14**, 354 (1996).
35. We thank D. Thiel, S. Gruner, and members of the MacCHESS staff for support and assistance in data collection at A1; J. Kuriyan, S. K. Burley, S. Harrison, P. Kim, E. Gouaux, and D. Wang for helpful discussions; Y. Jiang for help in data collection; D. Gadsby and J. Kuriyan for comments on the manuscript; and T. Rahman for patience and support. R.M. is forever grateful to T. Wiesel and A. L. MacKinnon for making this project possible. R.M. is an investigator of the Howard Hughes Medical Institute.

23 February 1998; accepted 13 March 1998

Classical Conditioning and Brain Systems: The Role of Awareness

Robert E. Clark and Larry R. Squire*

Classical conditioning of the eye-blink response, perhaps the best studied example of associative learning in vertebrates, is relatively automatic and reflexive, and with the standard procedure (simple delay conditioning), it is intact in animals with hippocampal lesions. In delay conditioning, a tone [the conditioned stimulus (CS)] is presented just before an air puff to the eye [the unconditioned stimulus (US)]. The US is then presented, and the two stimuli coterminate. In trace conditioning, a variant of the standard paradigm, a short interval (500 to 1000 ms) is interposed between the offset of the CS and the onset of the US. Animals with hippocampal lesions fail to acquire trace conditioning. Amnesic patients with damage to the hippocampal formation and normal volunteers were tested on two versions of delay conditioning and two versions of trace conditioning and then assessed for the extent to which they became aware of the temporal relationship between the CS and the US. Amnesic patients acquired delay conditioning at a normal rate but failed to acquire trace conditioning. For normal volunteers, awareness was unrelated to successful delay conditioning but was a prerequisite for successful trace conditioning. Trace conditioning is hippocampus dependent because, as in other tasks of declarative memory, conscious knowledge must be acquired across the training session. Trace conditioning may provide a means for studying awareness in nonhuman animals, in the context of current ideas about multiple memory systems and the function of the hippocampus.

Memory is composed of several different abilities that depend on different brain systems (*1*). A fundamental distinction is between the capacity for conscious recollection of facts and events (declarative or explicit memory) and various nondeclarative (implicit) forms of memory that are expressed in skills, habits, and simple forms of conditioning. This distinction is dramatically evident in amnesic patients, who have bilateral damage to the hippocampal formation or related midline diencephalic brain structures. These patients have severely impaired declarative memory and are profoundly forgetful. Yet these same patients have a fully intact capacity for nondeclarative memory (*2*). Indeed, a large body of literature involving both humans and experimental animals can now be understood by recognizing that memory tasks requiring declarative memory depend on the integrity of the hippocampal formation and related structures, whereas tasks requiring nondeclarative memory can be performed normally after damage to these structures and are supported by other brain systems. Declarative memory is what is meant by the term "memory" in ordinary language. It is involved in modeling the external world, and its contents can be brought to consciousness as a verbal proposition or as a mental image. By contrast, nondeclarative memory is expressed through performance without affording access to any conscious memory content or even awareness that memory is being used. This form of memory permits cumulative changes in perceptual and response systems and allows for the gradual development of new skills and habits.

A major puzzle about the distinction between conscious (hippocampus dependent) and nonconscious (hippocampus independent) forms of memory concerns classical conditioning. Classical conditioning, a phylogenetically early example of simple associative learning, has been studied extensively and would appear to be a quintessential example of nondeclarative memory (*3*). In perhaps the best studied classical conditioning paradigm, delay conditioning of the eye-blink response, a neutral conditioned stimulus (CS), such as a tone, is presented just before an air puff unconditioned stimulus (US). The US is then presented and the two stimuli coterminate (Fig. 1, A and B). Initially, an eye blink occurs reflexively in response to the US, but with repeated CS-US pairings a learned or conditioned response (CR) is elicited by the CS in advance of the US. The CR overlaps with the US such that the eye blink serves as an adaptive, defensive response to the air puff. Studies in the rabbit have shown that the cerebellum is essential for both the acquisition and retention of delay classical conditioning (*4*) and that no other forebrain structure, including the hippocampus, is required (*5*). Amnesic patients also exhibit intact acquisition and retention of the classically conditioned eye-blink response (*6*, *7*). Thus, eye-blink conditioning appears to have the automatic, reflexive features that are characteristic of nondeclarative memory.

The puzzle concerns trace conditioning, a slightly different version of classical conditioning in which the CS is presented and terminated and then a short interval is imposed before the presentation of the US (*8*) (Fig. 1, C and D). The name comes from the fact that the CS must leave some trace in the nervous system for a CS-US associ-

R. E. Clark is in the Department of Psychiatry, University of California, San Diego, La Jolla, CA 92093, USA. L. R. Squire is at the Veterans Affairs Medical Center, San Diego, CA 92161, USA, and Departments of Psychiatry and Neurosciences, University of California, San Diego, School of Medicine, La Jolla, CA 92093, USA.

*To whom correspondence should be addressed.

Evolution In Action

Emerging Insecticide Resistance in Mosquitoes

A three-dimensional molecular story about the acetylcholinesterase active site

Organophosphate insecticides are routinely used to control mosquito populations in areas where malaria is endemic. Many of these insecticides target the enzyme acetylcholinesterase --- which normally cleaves the acetylcholine neurotransmitter, and terminates synaptic transmission. A recent report by Weil et. al. (Nature, 423, pp136-137, 2003) described the molecular basis for this insecticide resistance --- a Gly119Ser mutation. Because it is difficult to communicate the close-packed nature of an enzyme active site, and the specific interactions between active site residues and the substrate/inhibitor with 2D illustrations and computer graphics, we have constructed a physical model of this enzyme active site.

This space-filled model of the active site "unfolds" to reveal the catalytic triad of active site residues Ser238, His480 and Glu367. The substrate and inhibitor can be alternatively docked into the active site. Replacement of the normal Gly119 sidechain with a serine sidechain blocks the binding of the insecticide, without interfering with substrate binding. This physical model is based on coordinates from 1qon.pdb.

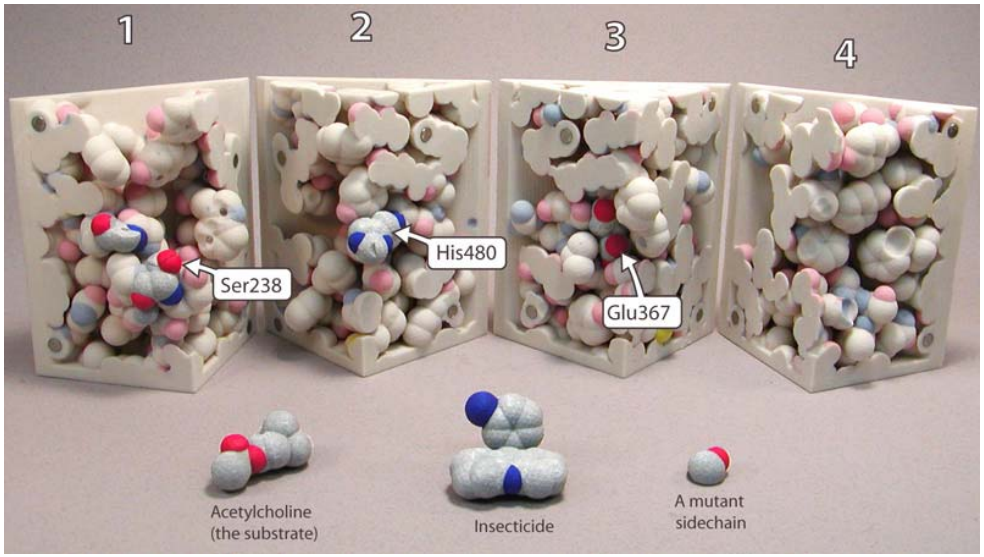

This model can be borrowed from the MSOE Model Lending Library.

MSOE Center for BioMolecular Modeling
...where teachers come first

www.msoe.edu/cbm

An NIH NCRR SEPA Project

June 2004: Acetylcholinesterase

Every time you move a muscle and every time you think a thought, your nerve cells are hard at work. They are processing information: receiving signals, deciding what to do with them, and dispatching new messages off to their neighbors. Some nerve cells communicate directly with muscle cells, sending them the signal to contract. Other nerve cells are involved solely in the bureaucracy of information, spending their lives communicating only with other nerve cells. But unlike our human bureaucracies, this processing of information must be fast in order to keep up with the ever-changing demands of life.

Neurotransmitters

Nerves communicate with one another and with muscle cells by using neurotransmitters. These are small molecules that are released from the nerve cell and rapidly diffuse to neighboring cells, stimulating a response once they arrive. Many different neurotransmitters are used for different jobs: glutamate excites nerves into action; GABA inhibits the passing of information; dopamine and serotonin are involved in the subtle messages of thought and cognition. The main job of the neurotransmitter acetylcholine is to carry the signal from nerve cells to muscle cells. When a motor nerve cell gets the proper signal from the nervous system, it releases acetylcholine into its synapses with muscle cells. There, acetylcholine opens receptors on the muscle cells, triggering the process of contraction. Of course, once the message is passed, the neurotransmitter must be destroyed, otherwise later signals would get mixed up in a jumble of obsolete neurotransmitter molecules. The cleanup of old acetylcholine is the job of acetylcholinesterase.

Acetylcholinesterase in Action

Acetylcholinesterase is found in the synapse between nerve cells and muscle cells. It waits patiently and springs into action soon after a signal is passed, breaking down the acetylcholine into its two component parts, acetic acid and choline. This effectively stops the signal, allowing the pieces to be recycled and rebuilt into new neurotransmitters for the next message. Acetylcholinesterase has one of the fastest reaction rates of any of our enzymes, breaking up each molecule in about 80 microseconds.

June 2004: Acetylcholinesterase

Electric Fish

Acetylcholinesterase was first studied by using the form found in electric fish, such as the torpedo ray. These fish have massive arrays of nerve-like structures in the organs that generate electricity, so acetylcholinesterase is particularly abundant. The form shown here, from PDB entry 1acj, forms a dimer in the crystal structure. It normally has lipids attached to the protein chains, which anchor the enzyme to the cell membrane. The lipids were removed in the crystal structure, however, to allow crystallization. The active site is found in a deep pocket, just big enough for the acetylcholine to slip down inside. At the base of the pocket is a triad of three amino acids--serine-histidine-glutamate.

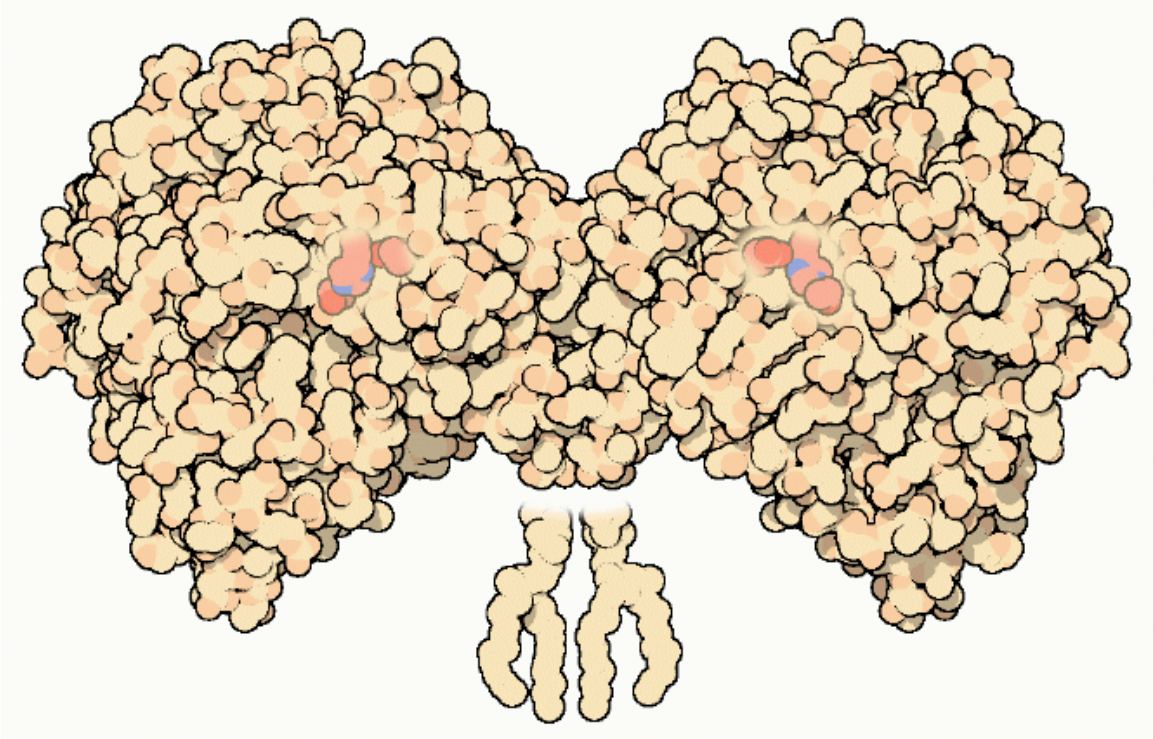

June 2004: Acetylcholinesterase

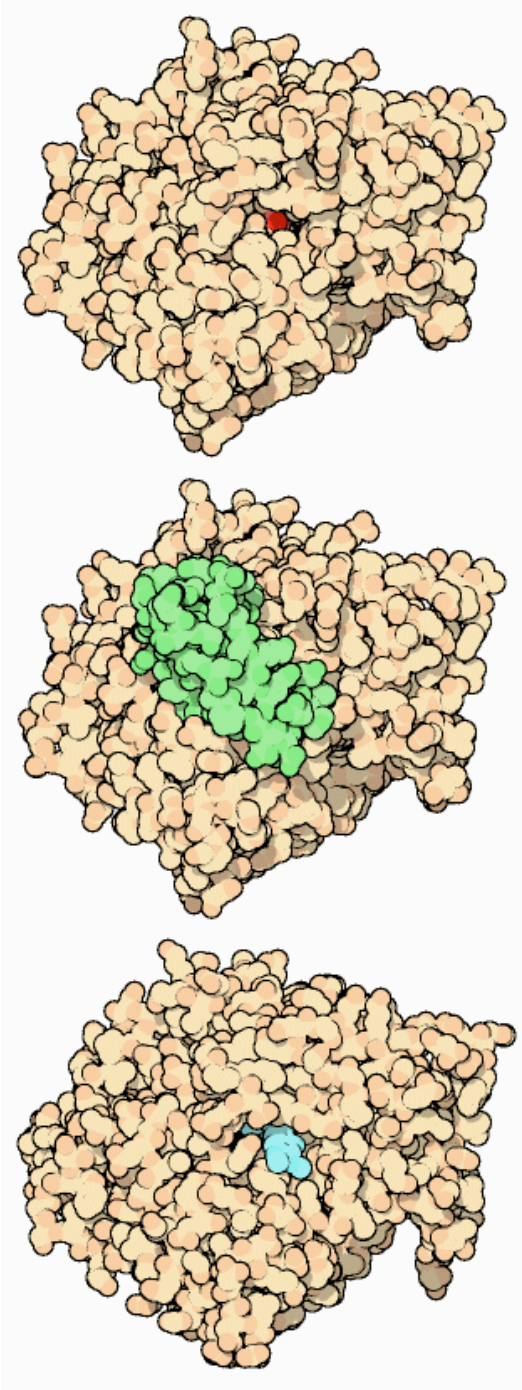

Attacking Acetylcholinesterase

Since acetylcholinesterase has an essential function, it is a potential weak point in our nervous system. Poisons and toxins that attack the enzyme cause acetylcholine to accumulate in the nerve synapse, paralyzing the muscle. Over the years, acetylcholinesterase has been attacked in many ways by natural enemies. For instance, some snake toxins attack acetylcholinesterase. The picture at the top shows a view straight down the active site tunnel, from PDB entry 1b41, showing the active site serine in red. The middle picture shows how a lethal toxin from the eastern green mamba blocks the active site and poisons the action of the enzyme.

Doctors are now willfully poisoning acetylcholinesterase in an attempt to reverse the symptoms of Alzheimer's disease. People with Alzheimer's disease lose many nerve cells as the disease progresses. By taking a drug that partially blocks acetylcholinesterase, the levels of the neurotransmitter can be raised, strengthening the nerve signals that remain. One drug being used in the way is shown at the bottom, from PDB entry 1eve. It inserts into the active site pocket and temporarily blocks entry of acetylcholine. Other poisons, as shown on the next page, take a more permanent approach.

June 2004: Acetylcholinesterase

Exploring the Structure

The nerve toxin sarin and insecticides such as malathion directly attack the active site machinery of acetylcholinesterase. The structure shown here, from PDB entry 1cfj, shows the active site triad of acetylcholinesterase after being poisoned by sarin. In the normal reaction, the serine amino acid forms a bond to the acetyl group of acetylcholine, breaking the molecule. Then, in a matter of microseconds, a water molecule breaks the new bond, releasing acetic acid and restoring the serine to its original form. Sarin, however, transfers a nasty methylphosphonate group (MeP in the picture) to the serine. The phosphonate is far more stable and will disable the enzyme for hours or days.

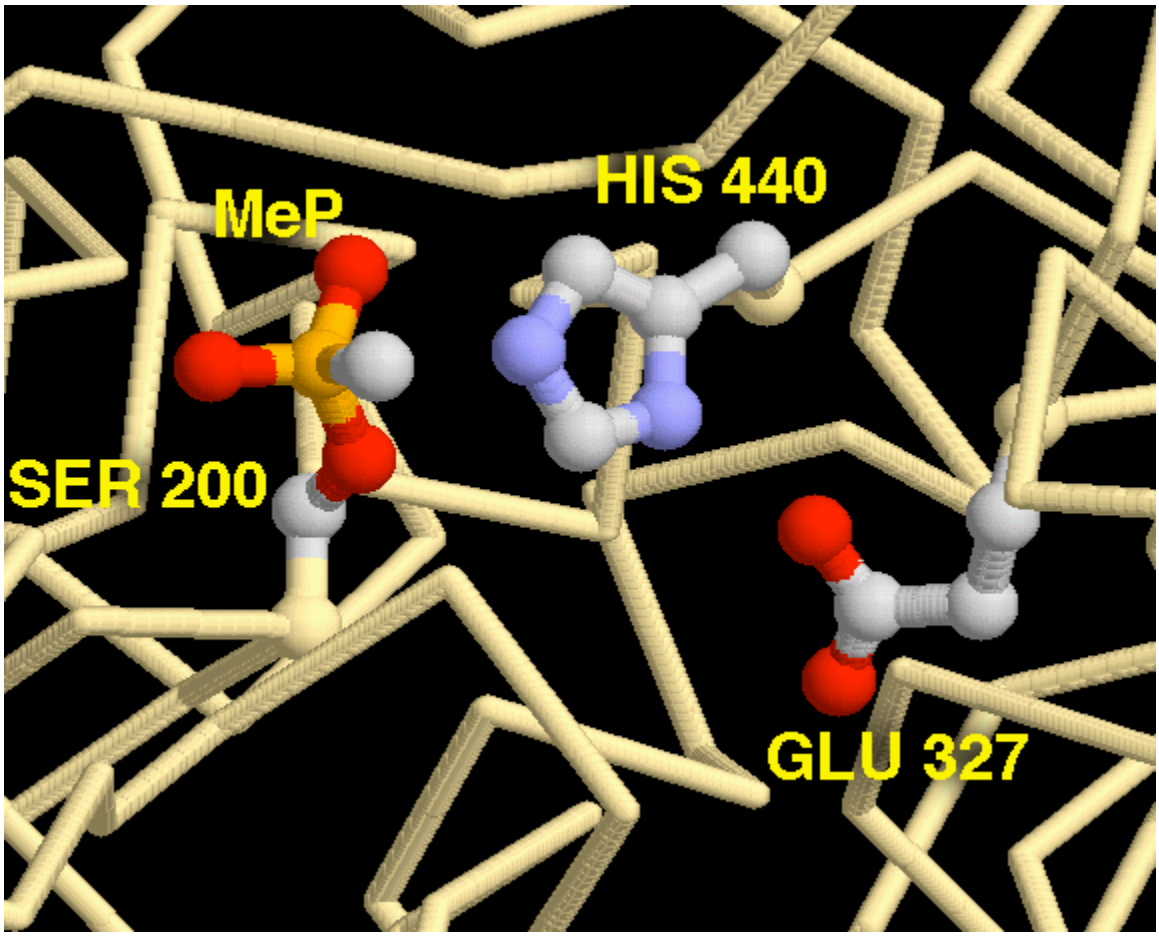

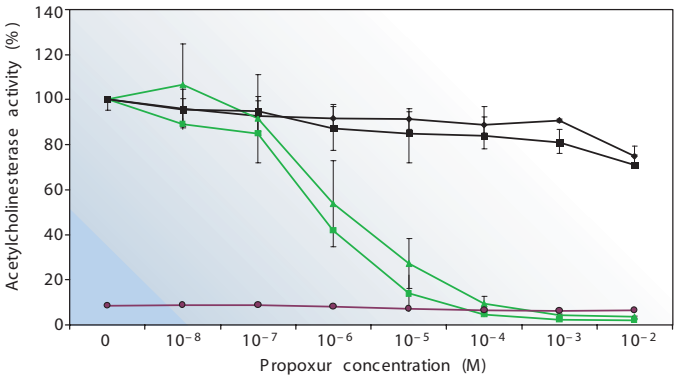

Figure 1 Residual acetylcholinesterase activity of susceptible (green squares) and resistant (black diamonds) mosquitoes assayed in homogenates and lysates from transfected S2 cells in the presence of increasing concentrations of the carbamate insecticide Propoxur. S2 cells were transfected with the recombinant pAc5.1/V5-His vector (Invitrogen) either alone (purple circles) or with expression of either sensitive acetylcholinesterase-1 (green triangles) or insensitive G119S-mutant enzyme (black squares). Residual enzyme activity was assayed after incubation with Propoxur for 15 min (ref. 5). Three independent experiments were carried out using different volumes of lysate. c

Comparative genomics

Insecticide resistance in mosquito vectors

Resistance to insecticides among mosquitoes that act as vectors for malaria (*Anopheles gambiae*) and West Nile virus (*Culex pipiens*) emerged more than 25 years ago in Africa, America and Europe; this resistance is frequently due to a loss of sensitivity of the insect's acetylcholinesterase enzyme to organophosphates and carbamates[1]. Here we show that this insensitivity results from a single amino-acid substitution in the enzyme, which we found in ten highly resistant strains of *C. pipiens* from tropical (Africa and Caribbean) and temperate (Europe) areas, as well as in one resistant African strain of *A. gambiae*. Our identification of this mutation may pave the way for designing new insecticides.

Acetylcholinesterase terminates synaptic transmission by hydrolysing the neurotransmitter acetylcholine; its inactivation by insecticides leads to paralysis and death. Mosquitoes, however, show widespread and strong resistance to this type of insecticide. They have two genes that encode different isoforms of acetylcholinesterase: *ace-1*, which has no homologue in the fruitfly *Drosophila melanogaster* and is closely linked to resistance in *C. pipiens*; and *ace-2*, a homologue of the unique *Drosophila ace* gene[2]. The generally mild insensitivity of acetylcholinesterase-2 in *D. melanogaster* is due to the combined weak effect of several mutations[3].

To identify mutations involved in resistance in mosquitoes, we determined the complete *ace-1* messenger RNA coding sequence of two *Culex pipiens* strains: one susceptible and one resistant (results not shown). *C. pipiens ace-1* encodes a putative 702-amino-acid protein, which is 81% identical to its *A. gambiae* homologue and 39% identical to *D. melanogaster* acetylcholinesterase-2. Complementary DNAs from the susceptible and resistant strains differ at 27 n cleotide positions, only one of which generates an amino-acid substitution: the GGC (glycine) codon at position 119, according to the nomenclature for *Torpedo* acetylcholinesterase[1], is replaced by an AGC (serine) codon in resistant mosquitoes (mutation G119S).

From three-dimensional modelling, we find that this mutated residue lies within the active 'gorge' of the enzyme, close to the catalytic site and abutting the oxyanion hole (results not shown). To evaluate the biochemical effect of the mutation *in vitro*, we assayed the catalytic properties and insecticidal sensitivity of wild-type and mutant recombinant acetylcholinesterase-1 that was expressed in S2 *Drosophila* cells. The G119S mutant showed the same insensitivity to Propoxur insecticide as resistant-strain acetylcholinesterase-1 (Fig. 1). A single mutation in *ace-1* must therefore be responsible for the insensitivity of the enzyme.

To determine whether the G119S mutation is present in other *C. pipiens* strains with insensitive acetylcholinesterase, we sequenced exon 3 of *ace-1* in several resistant and susceptible strains derived either from the temperate or the tropical/subtropical form of the *C. pipiens* species complex (*C. p. pipiens* and *C. p. quinquefasciatus*, respectively). All of the resistant strains carried the G119S substitution, regardless of their origin. Moreover, although 23 nucleotides were polymorphic, a unique haplotype was found to be associated with the resistance within each subspecies (see supplementary information). This indicates that the same G119S mutation has occurred independently at least twice in *C. pipiens*, once in each subspecies.

We also investigated the recent emergence of insensitive acetylcholinesterase in the main African malaria vector *Anopheles gambiae*[4], with the use of the *ace-1* genomic sequences of a resistant (YAO) and a susceptible (KISUMU) strain. The coding sequences differed at 18 nucleotide positions, two of them being non-synonymous. In the YAO strain, one mutation that resulted in the replacement of a valine residue by alanine in the amino-terminal region has no equivalent in *Torpedo* acetylcholinesterase and did not seem to affect the enzyme's catalytic properties (results not shown). The other was the same G119S substitution as in *C. pipiens* (results not shown), indicating that this single point mutation has occurred independently at least three times in the *ace-1* gene: twice in the *C. pipiens* complex and once in *A. gambiae*.

The discovery of the *ace-1* mutation that is responsible for insecticide resistance in mosquitoes opens the way to new strategies for pest management. The development of new insecticides that can specifically inhibit the G119S mutant form of acetylcholinesterase-1 will be crucial in overcoming the spread of resistance.

Mylène Weill*, Georges Lutfalla†, Knud Mogensen†, Fabrice Chandre‡, Arnaud Berthomieu*, Claire Berticat*, Nicole Pasteur*, Alexandre Philips§, Philippe Fort§, Michel Raymond*

**Institut des Sciences de l'Évolution (UMR 5554), CC 065, Université Montpellier II, 34095 Montpellier, France*
e-mail: weill@isem.univ-montp2.fr
†Défenses Antivirales et Tumorales (UMR 5124), and §Centre de Recherche en Biochimie des Macromolécules (UPR1086), CNRS, 34293 Montpellier, France
‡IRD/LIN, BP 64501, 34394 Montpellier, France

1. Toutant, J. P. *Progr. Neurobiol.* **32,** 423–446 (1989).
2. Weill, M. *et al. Proc. R. Soc. Lond. B* **269,** 2007–2016 (2002).
3. Mutéro, A., Pralavorio, M., Bride, J. M. & Fournier, D. *Proc. Natl Acad. Sci. USA* **91,** 5922–5926 (1994).
4. N'Guessan, R. *et al. Med. Vet. Entomol.* **17,** 1–7 (2002).
5. Bourguet, D., Pasteur, N., Bisset, J. & Raymond, M. *Pest. Biochem. Physiol.* **55,** 122–128 (1996).

Supplementary information accompanies this communication on *Nature*'s website.
Competing financial interests: declared none.

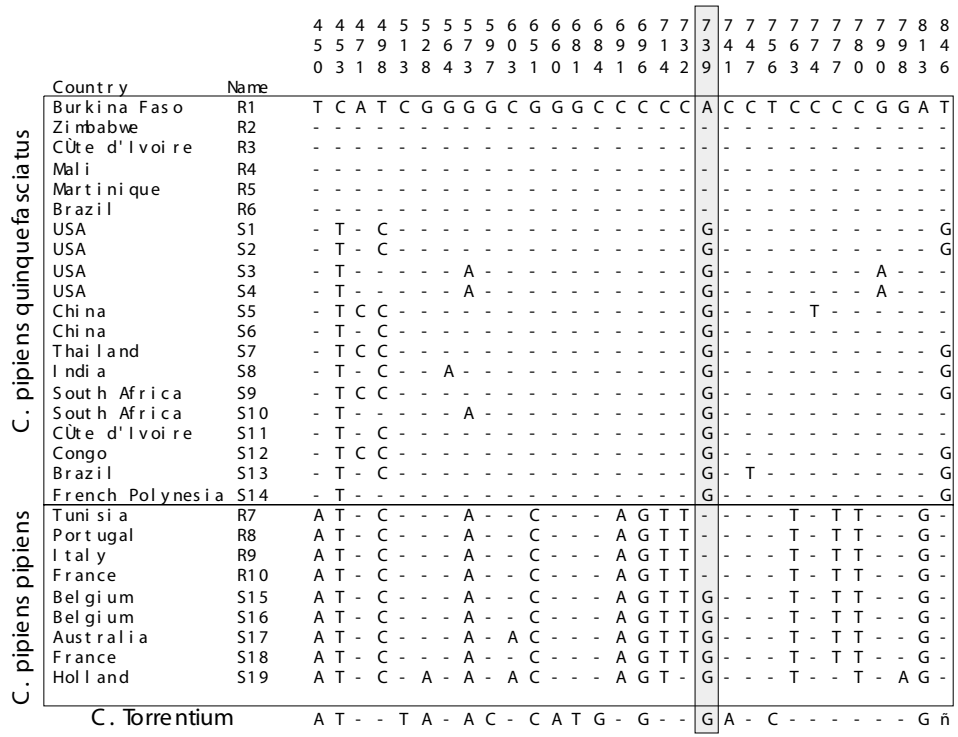

Figure S1. Nucleotide polymorphism in exon 3 of *ace-1* in *Culex pipiens* mosquitoes. Samples are listed according to subspecies (*C. p. pipiens* or *C. p. quinquefasciatus*), presence of insensitive AChE (Ri) or not (Si), and country of origin. Only polymorphic sites are indicated, and a dash indicates similarity with the top sequence. The position of the G119S mutation is boxed. *Culex torrentium*, the closest known species to the *C. pipiens* complex, is presented as an outgroup. See Supplementary Information for references for all samples.

Table S1. Name, country of origin and reference of the strains used in Figure S1.

Taxa	Name in Fig. S1	Real name	Country	Reference
C. p. quinquefasciatus	R1	BO	Burkina-Faso	M. Raymond, unpublished
	R2	HARARE	Zimbabwe	M. Raymond, unpublished
	R3	SUPERCAR	Côte d'Ivoire	1
	R4	DJI	Mali	M. Raymond, unpublished
	R5	MARTINIQUE	Martinique	2
	R6	RECIFE	Brazil	Collected in 1995 by A.-B. Failloux (Pasteur Institute, Paris, France)
	S1	PRO-R	USA	3
	S2	S-LAB	USA	3
	S3	TEM-R	USA	4
	S4	TRANS-P	USA	5
	S6	LING	China	6
	S7	MAO	China	7
	S6	THAI	Thailand	8
	S8	MADURAI	India	9
	S9	BSQ	South Arica	Collected in 1991 by A. J. Cornel (Sth Afr. Inst. Med. Res., South Africa)
	S10	BED	South Arica	Collected in 1991 by A. J. Cornel (Sth Afr. Inst. Med. Res., South Africa)
	S11	BOUAKE	Côte d'Ivoire	10
	S12	BRAZZA	Congo	11
	S13	BRESIL	Brazil	M. Raymond, unpublished
	S14	MOOREA	French Polynesia	12
C. p. pipiens	R7	ESPRO	Tunisia	13
	R8	PRAIAS	Portugal	14
	R9	PADOVA	Italy	15
	R10	BARRIOL	France	16
	S15	BRUGES-A	Belgium	17
	S16	BRUGES-B	Belgium	17
	S17	KILLCARE	Autralia	18
	S18	BLEUET	France	19
	S19	HETEREN	Holland	M. Raymond, unpublished
C. torrentium	-	UPPSALA	Sweden	20

1. Chandre, F. Thèse de Doctorat, Université Paris XII-Val de Marne (1998).
2. Bourguet, D., Raymond, M., Bisset, J., Pasteur, N. & Arpagaus, M. *Biochem. Genet.* **34**, 351-362 (1996).
3. Georghiou, G.P., Metcalf, R.L. & Gidden, F.E. *Bull. Wld Hlth Org.* **35**, 691-708 (1966).
4. Georghiou, G. & Pasteur, N. *J. Econ. Entomol.* **71**, 201-205 (1978).
5. Priester, T.M. & Georghiou, G.P. *J. Econ. Entomol.* **71**, 197-200 (1978).
6. Weill, M., *et al. Journal of the American Mosquito Control Association* **17**, 238-244 (2001).
7. Qiao, C.-L., Marquine, M., Pasteur, N. & Raymond, M. *Biochem. Genet.* **36**, 417-426 (1998).
8. Guillemaud, T., Rooker, S., Pasteur, N. & Raymond, M. *Heredity* **77**, 535-543 (1996).
9. Nielsen-Leroux, C., *et al. J. Med. Entomol.* **39**, 729-735 (2002).
10. Magnin, M., Marboutin, E. & Pasteur, N. *J. Med. Entomol.* **25**, 99-104 (1988).
11. Beyssat-Arnaouty, V. Thèse de Doctorat, Université de Montpellier II (1989).